University of West Bohemia
Faculty of Applied Sciences
Department of Mathematics

Diploma Thesis

Finite Volume Method for Radiative Heat Transfer Problems

Author: Aleš Pecka
Supervisor: Doc. Ing. Marek Brandner, Ph.D.
Date: May 2014

Declaration

I hereby declare that this thesis is the result of my own work and that all external sources of information have been duly acknowledged.

Plzeň, 21th May 2014 .....
Aleš Pecka

Acknowledgement

I would like to acknowledge and sincerely thank my supervisor, Doc. Ing. Marek Brandner, Ph.D., for his essential input and feedback during the writing of this thesis. I would not have been able to thoroughly express my understanding and research without his guidance and experience. No less thanks belong to Mgr. Ing. Ondřej Bublík for his valuable advice concerning especially the technical side of the problem.

Abstract

The equation of radiative transfer describes the transfer of energy in the form of electromagnetic radiation through absorbing, emitting and scattering medium. First of all, a derivation of the equation along with a description of the related physical processes is provided. The equation of radiative transfer is a space-time-direction-dependent integro-differential equation. In this thesis, both space and direction are discretised by the finite volume method. More specifically, a finite volume scheme for the two-dimensional case is derived using unstructured grid systems.

The main focus of the present thesis is the more atypical directional discretisation. The directional variable is discretised into a finite number of control angles, where the solution is approximated by constants. When evaluating the numerical flux on the boundary of a control volume, the problem that arises is that the flux might be incoming in one part of a control angle and outgoing in the other. Usually, the flux is approximated such that it is assumed to be either incoming or outgoing in the whole control angle. This is called the bold approximation. Here, a thorough manipulation of control angle overlap was chosen instead of the more common and less accurate bold approximation.

The derived scheme is tested on a few exemplary initial-boundary value problems. A numerical test of convergence is also preformed here.

Keywords

Radiative heat transfer, equation of radiative transfer, finite volume method, directional discretisation, exact treatment of control angle overlap.

Abstrakt

Transportní rovnice elektromagnetického záření popisuje přenos elektromagnetické energie médiem, které záření absorbuje, rozptyluje a samo i vyzařuje. Nejdříve jsou v této práci popsány tři zmíněné vlastnosti médií a následně odvozena transportní rovnice elektromagnetického záření. Tato rovnice je integro-diferenciální rovnicí s neznámou, která závisí na prostorové, časové i směrové proměnné. V této práci jsou směr i prostor diskretizovány metodou konečných objemů pro nestrukturované sítě ve dvoudimenzionálním případě.

Největší pozornost je kladena na neobvyklou diskretizaci směrové proměnné. Tuto proměnnou je třeba rozdělit na konečný počet úhlů, na kterých se uvažuje konstantní řešení. Na hraně prvku prostorové sítě se pak stává, že numerický tok na části úhlu vtéká do prvku a na jiné z něj vytéká. Toto se nejčastěji zjednodušuje tak, že se přepokládá, že numerický tok bud' vtéká nebo vytéká na celých oblastech jednotlivých úhlů (tedy i na těch hraničních). V této práci je každý hraniční úhel rozdělen na část vtékající a vytékající, což dává přesnější výsledky.

Odvozené schéma je prověřeno na několika počátečně-okrajových úlohách. Je zde také proveden numerický test konvergence.

Klíčová slova

Přenos tepelné radiace, transportní rovnice elektromagnetického záření, metoda konečných objemů, diskretizace směrové proměnné.

Contents

Chapter 1

Introduction

All non-ideal objects constantly emit and absorb electromagnetic radiation, thereby loosing or gaining some inner energy. The radiation emitted propagates through space at the speed of light until it is absorbed. This process is called radiative transfer and it differs from other forms of energy transfer mainly by its high speed of propagation and the fact that it can also take place inside a vacuum.

The absorptivity and emissivity of an object depends on its material, where the latter also depends on the object's temperature. In fact, the amount of emitted electromagnetic radiation increases substantially with a rising temperature. Radiative transfer, therefore, becomes an important process for applications that deal with high temperatures; examples of which include combustion in gas turbines, industrial glass cooling and photon radiotherapy. Electromagnetic radiation travels in straight lines through a vacuum, however, when propagating through a participating medium the radiation is constantly being scattered into other directions. An equation that describes the motion of electromagnetic radiation in participating media while taking emission, absorption and scattering into account, is called the equation of radiative transfer. We shall derive this equation in Chapter 2, wherein we also describe emission, absorption and scattering.

The equation of radiative transfer is an integral and first order differential equation, which differs from classical first order differential equations by its directional dependence. When numerically solving the equation, the directional variable must also be discretised. A number of approximation schemes have been developed for this purpose. In Chapter 3, we briefly describe two methods for the directional discretisation, namely the discrete ordinate method and the method of spherical harmonics. The latter is based on expressing the solution in Fourier series by means of spherical harmonic functions. Truncating the series may cause oscillations, especially for dis-

continuous initial and boundary conditions. The discrete ordinate method is a low order method, which replaces the uncountable number of directions with a finite number of carefully selected ones. This approach suffers from a number of defects, particularly from the so called ray effect.

In an attempt to reduce these defects the finite volume method has been employed to approximate direction. The central objective of the present thesis is to derive and apply the finite volume scheme to the equation of radiative transfer in both space and direction. We shall start off by introducing the standard finite volume method for the spatial discretisation in Chapter 4 along with numerical tests of convergence.

We shall preform the complete finite volume discretisation in Chapter 5 for unstructured triangulations in two-dimensional space. In this case, the direction is only one-dimensional. We will construct a partition with a finite number of control angles. The finite volume method is based on calculating an approximate solution that is piecewise constant with respect to the directional partition. The problem here is that on the edge of a control volume the flux may be incoming in one part of a control angle and outgoing in the other. In Chapter 5 we deal with the problem by splitting these control angles into the incoming and outgoing components. We will conclude this thesis by testing the scheme on a few initial-boundary value problems and preforming a numerical test of convergence. All the numerical results presented in this thesis were generated in Matlab, see [18].

Note, that the directional dependence is not exclusive to the radiative transfer equation. Another (and practically the only other) equation with this feature is the neuron transport equation. Neuron transport literature is thus also an excellent source of information for our purposes.

Chapter 2

Radiative transfer

Radiative transfer is a physical process where energy is transfered in the form of electromagnetic radiation. When electromagnetic radiation propagates through a participating medium, some of the radiation is absorbed, some scattered to other direction and the medium itself emits radiation. Thus, while mathematically describing radiative transfer, absorption, emission and scattering must be accounted for. The target of the present chapter is to derive the equation of radiative transfer. To this end, we will more or less follow Modest [13].

Every body with a temperature higher than absolute zero emits electromagnetic radiation. The amount of emitted energy depends on the temperature and the material of the body. Emission is therefore a process where inner energy of the body is transformed into electromagnetic radiation. Absorption on the other hand, is a phenomenon where electromagnetic radiation is transformed into inner energy of the medium, which typically results in an increase of temperature. This way electromagnetic radiation transfers heat from one place to another. This mechanism is called *radiative heat transfer* or *thermal radiation*. We may define thermal radiation as electromagnetic radiation of wavelengths roughly between 0.1 μm and 100 μm (mostly consist of infrared radiation), as the heat is transfered mostly in this range. To give an everyday example, the sun warms up all its surrounding planets including Earth by radiative heat transfer alone and the warmth that we feel coming out of a fire is caused by this process too. Using infrared vision we can see the heat which is emitted from animals and people in the form of infrared radiation.

There are two other mechanisms of heat transfer. One of them is what we call *conductive heat transfer*, where faster particles of a particular substance pass some of their kinetic energy to the slower ones through collisions. During this process the particles do not propagate through the substance, the

particles only oscillate around their centres of equilibrium. *Convective heat transfer* on the other hand is caused by the movement of fluids with various temperatures. Convection involves the combined processes of diffusion (scattering of molecules in different directions) and advection (transfer due to the fluid's bulk motion).

As electromagnetic radiation propagates also through vacuum, radiative heat transfer does not require the presence of a participating medium as apposed to conductive and convective heat transfer. Other differences between conductive and convective heat transfer on the one hand and radiation heat transfer on the other are their ranges of impact, speeds of propagation and temperature dependences. A photon travels at high velocity known as the speed of light and its path can be as short as 10^{-10} m before being absorbed or it can travel as long as 10^{10} m (e.g. the sun rays hitting Earth). Radiation heat transfer is therefore a long-range phenomenon in general. Conduction and convection are on the other hand short-range phenomena with the speed of propagation insignificant to the speed of light. Conductive and convective heat transfer rates are usually assumed to be linearly proportional to the temperature whereas radiative heat transfer rates are generally proportional to difference in temperature to the fourth power. Hence, radiative heat transfer becomes more significant with rising temperature and may even become dominant over conductive and convective heat transfer. For these reasons, the study of radiative heat transfer is of great importance in vacuum or when high temperatures are involved, which occurs for instance in astrophysics and space applications. Concrete applications include photon radiotherapy [6], combustion in gas turbines [17] and so forth.

2.1 Properties of electromagnetic radiation

Electromagnetic radiation is a form of energy which can be viewed as propagating through space via either electromagnetic waves, or stream of photons. The latter is the view of quantum mechanics, whereas electromagnetic waves are predicted by electromagnetic wave theory. Neither of the two views can describe the observed behaviour completely and neither has been found more valid then the other. Therefore, they are being used interchangeably in the scientific community. The speed of light c [m/s] (the velocity of electromagnetic waves) depends on the medium in which it travels. It can be related to the speed of light in vacuum c_0 by the equality

$$c = \frac{c_0}{n_c}, \qquad c_0 \doteq 2.998 \cdot 10^8 \left[\frac{\mathrm{m}}{\mathrm{s}}\right],$$

where $n_c \geq 1$ is the *refractive index* of the medium. Electromagnetic waves can be determined by any of the following quantities

$$\begin{aligned}&\text{frequency } \nu \text{ [s}^{-1}\text{]},\\ &\text{wavelength } \lambda \text{ [m]},\\ &\text{wavenumber } \eta \text{ [m}^{-1}\text{]}.\end{aligned}$$

The quantities are related by the formulas

$$\nu = \frac{c}{\lambda} = c\eta.$$

A photon caries energy ϵ [J] that is directly proportional to the frequency of its associated electromagnetic wave, with Planck's constant h_P as the proportionality constant, that means

$$\epsilon = h_P \nu, \qquad h_P \doteq 6.626 \cdot 10^{-34} [\text{J s}].$$

The energy of an electron stays unchanged when entering a new medium. Thus, the frequency of the electron's associated electromagnetic wave also remains constant, while wavelength and wavenumber change depending on refractive indexes of the two neighbouring media.

2.2 Radiance and irradiance

Radiance is radiative energy transferred per unit time, unit solid angle and unit area perpendicular to the beam of electromagnetic radiation. *Spectral radiance* I is radiance per unit spectral variable. From now on, we will be using spectral radiance to describe the radiative transfer, as it is the most appropriate variable for this purpose. Spectral radiance is a function of location, direction, spectral variable and time. In the most general case, spectral radiance is 7-dimensional, with three spatial, two directional, one spectral and one temporal dimensions. Let us note that radiance is often confusingly called intensity. We will avoid using this terminology as the most common meaning for intensity in physics is energy transfered per unit time and area.

Furthermore, we introduce *irradiance*, which is radiative energy transferred per unit time and unit area perpendicular to the beam. *Spectral irradiance* E is analogically defined as irradiance per unit spectral variable. Spectral irradiance is a function of location, spectral variable and time. Spectral irradiance will be especially helpful when depicting the numerical results. In some literature, irradiance is also called intensity.

We will be using only the spectral versions of the quantities above. Let us sum up their definitions

$$\text{spectral radiance } I = \frac{\text{energy}}{\text{time * solid angle * spectral variable * proj. area}},$$
$$\text{spectral irradiance } E = \frac{\text{energy}}{\text{time * spectral variable * projected area}}.$$

Radiance and irradiance are related through

$$E = \int_{4\pi} I \; d\Omega.$$

and their dependence is as follows

$$I = I(\mathbf{r}, \mathbf{s}, t),$$
$$E = E(\mathbf{r}, t),$$

where $\mathbf{r}$ is the location vector, $\mathbf{s}$ is the unit directional vector, and t is time. Both radiance and irradiance also depend on the spectral variable λ (or ν or η). As we will see later, the equation of radiative transfer is not coupled with respect to the spectral variable, hence we will always hide its dependence from the view for simplicity. Moreover, whenever we talk about radiance and irradiance in this thesis, we actually refer to the spectral radiance and spectral irradiance.

2.3 Black body

When a beam of electromagnetic radiation hits a surface of a medium, some of the radiation may be reflected and the rest penetrates into the medium. We refer to an idealised physical body that absorbs all incident electromagnetic radiation, regardless of frequency or angle of incidence, as a *black body*. The amount of emitted electromagnetic radiation of a black body follows Planck's law which stays that

$$B_\lambda(T, \lambda) = 2h_P c^2 \lambda^{-5} \left[\exp\left(\frac{h_\mathrm{P} c}{\lambda k_B T} \right) - 1 \right]^{-1}, \tag{2.1}$$

or

$$B_\nu(T, \nu) = 2h_P c^{-2} \nu^3 \left[\exp\left(\frac{h_\mathrm{P} \nu}{k_B T} \right) - 1 \right]^{-1}, \tag{2.2}$$

or

$$B_\eta(T,\eta) = 2h_P c^2 \eta^3 \left[\exp\left(\frac{h_P c \eta}{k_B T}\right) - 1\right]^{-1}, \tag{2.3}$$

where Planck's function B_λ (or B_ν or B_η) is the spectral radiance of electromagnetic radiation that is emitted by the black body in all directions, T is temperature of the body and k_B is the Boltzmann constant with the value of

$$k_B \doteq 1.3807 \cdot 10^{-23} \left[\frac{\mathrm{J}}{\mathrm{K}}\right].$$

Let us remind that h_P is the Planck's constant, c is the speed of light and λ, ν and η are spectral variables. It follows that the emitted energy by a black body at a specific frequency depend on the body's temperature alone and remains constant in all directions. It can be shown (see [13], Section 1.3) that a black body is an ideal emitter, which means that it emits as much or more energy at every frequency than any other body at the same temperature.

2.4 Absorption, emission and scattering

Consider a beam of electromagnetic radiation traveling in a vacuum in the direction $\mathbf{s}$. Its spectral radiance in the direction $\mathbf{s}$ remains constant along its path (see [13], Section 9.2). On the other hand, when the beam propagates through a participating medium, absorption, emission and scattering play its role. In this section, we shall derive the equation of radiative transfer which mathematically describes propagation of electromagnetic radiation through absorbing, emitting and scattering medium. We choose λ as the spectral variable.

If a medium has a constant refractive index, then electromagnetic waves propagate through the medium along straight lines. On the other hand, changing refractive index would cause bending of the beam. In the following, we always consider only media with constant refractive index. Furthermore, we assume that the media are non-polarising and at local thermodynamic equilibrium.

2.4.1 Absorption and emission

A beam that travels through a participating medium is constantly attenuated by absorption and scattering. We will discuss scattering in the next section. Absorption is a process where electromagnetic energy is taken up by matter and transformed into internal energy. It has been discovered that the amount

of absorbed energy, with spectral radiance I_{a}, is directly proportional to the spectral radiance I of the beam and to the distance ℓ which the beam travels through medium. This can be written as

$$dI_{\mathrm{a}} = \sigma_{\mathrm{a}} I \; d\ell. \tag{2.4}$$

The proportionality constant σ_{a} is known as *the absorption coefficient* and is a function of the spectral variable with units of inverse length. The absorption coefficient depends on the material of the medium.

Every body with a temperature higher than absolute zero emits electromagnetic radiation. In the previous section, we explained that the radiance of electromagnetic radiation emitted by black body is given by Planck's function. Real materials emit electromagnetic radiation at a fraction, called *the emission coefficient*, of black-body emissivity (measured by means of its radiance). Using the fact that in thermodynamic equilibrium, the overall radiance must be equal to the radiance of a black body, it can be shown that the emission coefficient is the same as the absorption coefficient (see [13], Section 10.2, equation (10.16)). Thus, we can write

$$dI_{\mathrm{e}} = \sigma_{\mathrm{a}} B \; d\ell, \tag{2.5}$$

where I_{e} is spectral radiance of the emitted electromagnetic radiation in the same direction as I and $B = B_\lambda(T, \lambda)$ is Planck's function as defined in (2.1). If we chose ν or η as the spectral variable, we would take (2.2) or (2.3) as Planck's function instead. Combining (2.4) and (2.5) leads us to an equation describing spectral radiance of electromagnetic radiation in absorbing and emitting medium, namely

$$\frac{dI}{d\ell} = \sigma_{\mathrm{a}}(B - I).$$

2.4.2 In-scattering and out-scattering

Attenuation due to scattering or out-scattering is a process where a part of electromagnetic radiation is redirected from the considered direction into other directions, where it appears as augmentation. Again, the magnitude of scattered electromagnetic radiation, with spectral radiance I_{out}, is directly proportional to I and ℓ. This gives the expression

$$dI_{\mathrm{out}} = \sigma_{\mathrm{s}} I \; d\ell, \tag{2.6}$$

with *the scattering coefficient* σ_{s} as the proportionality constant. Just as the absorption coefficient, the scattering coefficient is a function of the spectral

variable with units of inverse length and it is associated with the material of the medium.

The equation (2.6) determines the amount of electromagnetic radiation that is scattered away from the considered direction, say $\mathbf{s}$. We shall develop a relation which describes the electromagnetic radiation that is scattered from other directions into $\mathbf{s}$. This process is called augmentation by scattering or in-scattering.

Electromagnetic radiation does not necessarily need to be scattered uniformly to all directions (that is a special case called isotropic scattering). For this reason we introduce *the scattering face function* Ψ which prescribes rate $\Psi(\mathbf{s}_1, \mathbf{s}_2)/4\pi$ (to any two directions $\mathbf{s}_1$ and $\mathbf{s}_2$) by which electromagnetic radiation is scattered from $\mathbf{s}_1$ into $\mathbf{s}_2$. Moreover, Ψ must obeys the integral identity

$$\frac{1}{4\pi} \int_{4\pi} \Psi(\mathbf{s}_1, \mathbf{s}_2)\ d\Omega_2 = 1. \tag{2.7}$$

The constant $1/4\pi$ is introduced in order for the integral identity to be true if $\Psi \equiv 1$ (which is the mentioned isotropic scattering). We will explain the reason for the condition (2.7) later.

Multiplying the right-hand side of (2.6) by the rate $\Psi(\mathbf{s}', \mathbf{s})/4\pi$ gives us the spectral radiance $I_{\mathbf{s}' \to \mathbf{s}}$ of electromagnetic radiation scattered from the direction $\mathbf{s}'$ into $\mathbf{s}$, namely

$$dI_{\mathbf{s}' \to \mathbf{s}} = \frac{\sigma_\mathrm{s}}{4\pi} \Psi(\mathbf{s}', \mathbf{s}) I(\mathbf{r}, \mathbf{s}', t)\ d\ell. \tag{2.8}$$

To add up contributions from all directions, we simply integrate the equality over the unit sphere with respect to $\mathbf{s}'$, thereby obtaining

$$dI_\mathrm{in} = \frac{\sigma_\mathrm{s}}{4\pi} \int_{4\pi} \Psi(\mathbf{s}', \mathbf{s}) I(\mathbf{r}, \mathbf{s}', t)\ d\Omega'\ d\ell. \tag{2.9}$$

Here I_in is in-scattering, in other words the spectral radiance of electromagnetic radiation scattered from all direction into the direction $\mathbf{s}$. Notice that the relation for in-scattering is considerably more complicated than the relations for absorption, emission or out-scattering. In fact, the term (2.9) is the only one that couples all directions together, therefore prevents us from considering each direction separately.

Let us explain the reason for the condition (2.7). Integrating (2.8) over the unit sphere with respect to $\mathbf{s}$ gives us spectral radiance of all the electromagnetic radiation that is scattered away from $\mathbf{s}'$. That is nothing else

than out-scattering which is already described by (2.6). This lead us to the requirement

$$\frac{\sigma_{\mathrm{s}}}{4\pi}\int_{4\pi}\Psi(\mathbf{s}',\mathbf{s})\;d\Omega\;I(\mathbf{r},\mathbf{s}',t)\;d\ell=\sigma_{\mathrm{s}}I(\mathbf{r},\mathbf{s}',t)\;d\ell.$$

We obtain the condition (2.7) by dividing the equation by $\sigma_{\mathrm{s}}I(\mathbf{r},\mathbf{s}',t)\;d\ell$.

2.5 Equation of radiative transfer

We shall derive the radiative transfer equation in a slightly different manner than Modest [13]. We make an energy balance on a beam traveling from $\mathbf{r}_1$ to $\mathbf{r}_2$ in the direction $\mathbf{s}$ which leaves $\mathbf{r}_1$ at time t_1. Let the beam reaches $\mathbf{r}_2$ at time t_2 and let $\ell_{12}=||\mathbf{r}_1-\mathbf{r}_2||$ denote the distance between $\mathbf{r}_1$ and $\mathbf{r}_2$. We obtain the change in radiance I_Δ by summing augmentation by emission (2.5) and in-scattering (2.9) and subtracting the attenuation by absorption (2.4) and out-scattering (2.6), i.e.

$$I_\Delta=I_{\mathrm{e}}-I_{\mathrm{a}}-I_{\mathrm{out}}+I_{\mathrm{in}}.$$

Integrating I_Δ over the distance between $\mathbf{r}_1$ and $\mathbf{r}_2$ we receive the change in radiance between the points $\mathbf{r}_1$ and $\mathbf{r}_2$ (hence also between the times t_1 and t_2), namely

$$\begin{aligned}I(\mathbf{r}_2,\mathbf{s},t_2)-I(\mathbf{r}_1,\mathbf{s},t_1)&=\int_0^{\ell_{12}}dI_\Delta=\int_0^{\ell_{12}}(dI_{\mathrm{e}}-dI_{\mathrm{a}}-dI_{\mathrm{out}}+dI_{\mathrm{in}})\\&=\int_0^{\ell_{12}}\left[\sigma_{\mathrm{a}}B-(\sigma_{\mathrm{a}}+\sigma_{\mathrm{s}})I(\mathbf{r},\mathbf{s},t)+\frac{\sigma_{\mathrm{s}}}{4\pi}\int_{4\pi}\Psi(\mathbf{s}',\mathbf{s})I(\mathbf{r},\mathbf{s}',t)\;d\Omega'\right]d\ell.\end{aligned}\tag{2.10}$$

Electromagnetic radiation travels in straight lines at the speed of light c, therefore the functions

$$\begin{aligned}\mathbf{r}(\ell)&=\mathbf{r}_1+\ell\mathbf{s},\\t(\ell)&=t_1+\frac{\ell}{c},\end{aligned}$$

describe respectively the position and time of the beam at the distance ℓ from $\mathbf{r}_1$. Clearly we have

$$\begin{aligned}\mathbf{r}(0)&=\mathbf{r}_1, & \mathbf{r}(\ell_{12})&=\mathbf{r}_2,\\t(0)&=t_1, & t(\ell_{12})&=t_2.\end{aligned}$$

Assuming that radiance I has the spatial derivative in the direction $\mathbf{s}$ and the time derivative along the line between $\mathbf{r}_1$ and $\mathbf{r}_2$, we rewrite the very left-hand side of (2.10) as follows

$$\begin{aligned} I(\mathbf{r}_2,\mathbf{s},t_2) - I(\mathbf{r}_1,\mathbf{s},t_1) &= I\big(\mathbf{r}(\ell_{12}),\mathbf{s},t(\ell_{12})\big) - I\big(\mathbf{r}(0),\mathbf{s},t(0)\big) \\ &= \int_0^{\ell_{12}} \frac{dI}{d\ell}(\mathbf{r},\mathbf{s},t)\ d\ell = \int_0^{\ell_{12}} \left[\mathbf{s}\nabla I(\mathbf{r},\mathbf{s},t) + \frac{1}{c}\frac{\partial I}{\partial t}(\mathbf{r},\mathbf{s},t)\right] d\ell, \end{aligned}$$

where we hide the dependence of $\mathbf{r} = \mathbf{r}(\ell)$ and $t = t(\ell)$ on ℓ for transparency. We employed the chain rule in the last equality. Plugging the received expression into (2.10) we derive the integral energy balance

$$\int_0^{\ell_{12}} \left[\mathbf{s}\nabla I + \frac{1}{c}\frac{\partial I}{\partial t}\right] d\ell = \int_0^{\ell_{12}} \left[\sigma_{\mathrm{a}} B - (\sigma_{\mathrm{a}} + \sigma_{\mathrm{s}}) I + \frac{\sigma_{\mathrm{s}}}{4\pi} \int_{4\pi} \Psi(\mathbf{s}',\mathbf{s}) I(\mathbf{r},\mathbf{s}',t)\ d\Omega'\right] d\ell.$$

Whenever we do not show the dependence of I, we assume $I = I(\mathbf{r},\mathbf{s},t)$. Applying the mean value theorem to the integrals on either side of the equation, while assuming continuity of the integrands, leads us to the differential form of the energy balance, namely

$$\frac{1}{c}\frac{\partial I}{\partial t} + \mathbf{s}\nabla I = \sigma_{\mathrm{a}} B - (\sigma_{\mathrm{a}} + \sigma_{\mathrm{s}}) I + \frac{\sigma_{\mathrm{s}}}{4\pi} \int_{4\pi} \Psi(\mathbf{s}',\mathbf{s}) I(\mathbf{r},\mathbf{s}',t)\ d\Omega'. \tag{2.11}$$

This equation, called the equation of radiative transfer, is the central equation of the whole thesis. The unknown function is spectral radiance $I = I(\mathbf{r},\mathbf{s},t)$ which also depends on the spectral variable λ, however the equation is not coupled with respect to this variable. Therefore, we can solve the equations for each value of λ separately and so we do not explicitly show the spectral variable. The material coefficients σ_{a} and σ_{s} also depend on the spectral variable and may vary with location, since rays may penetrate through different media consisting of different materials. Planck's function $B = B_\lambda(T,\lambda)$, defined by (2.1), depends on temperature $T = T(\mathbf{r},t)$ and the spectral variable. Let us sum up the dependences:

$$\begin{aligned} \sigma_{\mathrm{a}} &= \sigma_{\mathrm{a}}(\mathbf{r},\lambda), \\ \sigma_{\mathrm{s}} &= \sigma_{\mathrm{s}}(\mathbf{r},\lambda), \\ B &= B_\lambda(T,\lambda), \\ T &= T(\mathbf{r},t). \end{aligned}$$

Note that in this section we use λ, however we may substitute it for an alternative spectral variable ν or η or even for energy $\epsilon = h_{\mathrm{P}}\nu$, if it is more convenient. We then also must substitute Planck's function for B_ν or B_η, which are defined by (2.2) or (2.3), respectively.

In the present thesis, we do not deal with realistic boundary conditions for the equation of radiative transfer. Instead, we consider only non-reflective wall, also called the black surface. In this case, we have the Dirichlet boundary condition (for incoming radiance) given by external radiation and emission of the wall. Boundary conditions for a number of reflective surfaces were described by Modest (see [13], Section 9.7).

Temperature field

A question that arises is where we get the temperature field $T = T(\mathbf{r}, t)$, which we need to plug into Planck's function. We assumed that the change in temperature due to all processes other than radiative heat transfer (convective and conductive heat transfer) is given. In general, electromagnetic radiation also influences temperature. During absorption, electromagnetic radiation transforms into inner energy of the material, which results in the increase of temperature. Emission on the other hand is the opposite process. This phenomenon is described by the so called material energy equation, which forms a coupled system with the equation (2.11), the radiative transfer equation.

If the heating and cooling of the material due to absorption and emission of electromagnetic radiation is small, we can neglect it and consider only the given change in temperature. In this thesis, we always assume the temperature given, hence we do not solve the material energy equation.

Cold medium

Typically, if the temperature of a body is low, then the amount of emitted electromagnetic radiation by the body is also relatively low. Hence, when electromagnetic radiation propagates through a cold medium, the amount of emitted electromagnetic radiation may be negligible compare to the amount of incoming electromagnetic radiation. This means that $B \approx 0$ and the first term on the right-hand side of the equation (2.11) disappears. In this case, the dependence of the radiative transfer equation on temperature vanishes completely.

Assumptions

We made a number of simplifications during the development of the equation of radiative transfer. We assume that the refractive index is constant and that the medium is at local thermal equilibrium. Moreover, we consider only homogeneous and non-polarising media that are at rest in comparison with the speed of light. Radiation transfer equation for a medium with varying refractive index was given by Pomraning [16].

Chapter 3

Directional approximation

In this chapter, we introduce a few methods that approximate direction in directional dependent equations and demonstrate them on the equation of radiative transfer, which we derived in the previous chapter in the form (2.11), namely

$$\frac{1}{c}\frac{\partial I}{\partial t} + \mathbf{s}\nabla I = \sigma_{\mathrm{a}} B - (\sigma_{\mathrm{a}} + \sigma_{\mathrm{s}})I + \frac{\sigma_{\mathrm{s}}}{4\pi}\int_{4\pi} \Psi(\mathbf{s}', \mathbf{s}) I(\mathbf{r}, \mathbf{s}', t)\ d\Omega'. \tag{3.1}$$

To be specific, we will introduce the discrete ordinate method, the method of spherical harmonics and the diffusion method. We shall devote it a separate chapter to the finite volume method, as it is the centre of focus of the present thesis.

The target of the methods mentioned above is essentially to approximate a directional dependent equation with a system of equations independent of direction. We can then solve the received equations by standard methods for partial differential equations. A brief introduction to the methods as well as their comparison in the form of numerical experiments was preformed by Brunner [1]. More thorough description of these methods was given by Modest [13].

Notation

For a natural number k a k-th moment is defined as $\int_{4\pi}(\mathbf{s} \otimes \mathbf{s} \otimes \ldots \otimes \mathbf{s})\ d\Omega$ and the k-th moment of an arbitrary function f is $\int_{4\pi}(\mathbf{s} \otimes \mathbf{s} \otimes \ldots \otimes \mathbf{s}) f\ d\Omega$, where we have $k-1$ outer products $\otimes$ in both expressions. Note that an outer product operates on two vectors to yield a tensor. We analogically define the zeroth moment as $\int_{4\pi} d\Omega$. The zeroth, first and second moments

satisfy

$$\int_{4\pi} d\Omega = 4\pi, \tag{3.2}$$

$$\int_{4\pi} \mathbf{s}\ d\Omega = 0, \tag{3.3}$$

$$\int_{4\pi} \mathbf{s} \otimes \mathbf{s}\ d\Omega = \frac{4\pi}{3}\mathbb{I}, \tag{3.4}$$

with the identity tensor $\mathbb{I}$. The first equality is obvious, for the other two see [Modest [13], Section 15.14, equations (15.27) and (15.29)]. It follows that irradiance E is the zeroth moment of radiance I. Let us define the radiative flux $\mathbf{F}$ as the first moment and radiation pressure tensor $\mathbb{P}$ as the second moment of I. To sum up we have

$$E = \int_{4\pi} I\ d\Omega,$$

$$\mathbf{F} = \int_{4\pi} \mathbf{s}\ I\ d\Omega, \tag{3.5}$$

$$\mathbb{P} = \int_{4\pi} (\mathbf{s} \otimes \mathbf{s}) I\ d\Omega. \tag{3.6}$$

3.1 Discrete ordinate method

In this section, we will derive *the discrete ordinate method*, which comes from a simple idea, which is to consider only a finite number of directions and ignore the rest. This method is famous for its simplicity, however it suffers from several unphysical numerical side effects, which are to be covered in Section 3.3. The method of discrete ordinates was first proposed by Chandrasekhar [2].

As we already mentioned, the discrete ordinate method assumes that particles can only travel along several particular direction. This approximation reduces the direction dependent equation of radiative transfer into a system of differential equation each of which is independent of direction. The discrete ordinate method can be viewed as the finite difference method employed to the directional variable with additional requirements. For instance, if we desire for the approximation to conserve energy, we cannot choose the directions arbitrarily, the directions along with their associated quadrature

weights must satisfy some additional conditions. Furthermore, the directions and weights are typically chosen to be invariant to any ninety degree rotation. The discrete ordinate method is also described by Modest [13] for the radiative transfer equation or by Lee [10] for problems in neutron transport theory.

Let us assume that $\mathbf{s}_1, \mathbf{s}_2, \ldots, \mathbf{s}_M$ are arbitrary unit directional vectors and $w_1, w_2, \ldots, w_M$ are their associated quadrature weights. We will discuss the particular choice of directions and quadrature weights in Section 3.1.1. Since the radiative transfer equation is integro-differential equation, we need to approximate the integral describing in-scattering. In general, if f is an arbitrary function of direction, we approximate its integral by the numerical quadrature

$$\sum_{m=1}^{M} w_m f(\mathbf{s}_m) \approx \int_{4\pi} f(\mathbf{s}) \, d\Omega. \tag{3.7}$$

We denote the approximation of the spectral radiance I in the direction $\mathbf{s}_m$ by I_m, where $m \in \{1, \ldots, M\}$, i.e.

$$I_m(\mathbf{r}, t) \approx I(\mathbf{r}, \mathbf{s}_m, t). \tag{3.8}$$

Considering only the directions $\mathbf{s}_1, \mathbf{s}_2, \ldots, \mathbf{s}_M$ and applying the quadrature rule (3.7) to the integral in (3.1) we obtain the discrete ordinate scheme for the equation of heat transfer, namely the system

$$\frac{1}{c}\frac{\partial I_m}{\partial t} + \mathbf{s}_m \nabla I_m = \sigma_\mathrm{a} B_\lambda - (\sigma_\mathrm{a} + \sigma_\mathrm{s}) I_m + \frac{\sigma_\mathrm{s}}{4\pi} \sum_{n=1}^{M} \Psi(\mathbf{s}_n, \mathbf{s}_m) I_n, \tag{3.9}$$

for all $m \in \{1, 2, \ldots, M\}$. Each of the M linear differential equations of the above system is independent of the directional variable. Hence, the system can be solved by standard method for partial differential equations. Note that the system (3.9) is coupled through the sum on the right-hand side which arises from the in-scattering term.

For many problem, only irradiance E is important and radiance I is used only to calculate it. When (3.9) is solved, irradiance can be approximated by $I_1, I_2, \ldots, I_M$ as

$$E = \int_{4\pi} I \, d\Omega \approx \sum_{m=1}^{M} w_m I_m.$$

3.1.1 Choice of directions and quadrature weights

As we have already noted, it is desirable for us to choose symmetrical directions and quadrature weights, so that they are invariant to any ninety degree rotation. We shall demand the zeroth, first and second moments to be satisfied, that is

$$\begin{aligned}
\int_{4\pi} d\Omega &= 4\pi &&= \sum_{m=1}^{M} w_m, \\
\int_{4\pi} \mathbf{s}\, d\Omega &= 0 &&= \sum_{m=1}^{M} w_m \mathbf{s}_i, \\
\int_{4\pi} \mathbf{s} \otimes \mathbf{s}\, d\Omega &= \frac{4\pi}{3}\mathbb{I} &&= \sum_{m=1}^{M} w_m \mathbf{s}_i \mathbf{s}_i^T.
\end{aligned}$$

Various sets of directions and weight satisfying the above conditions are tabulated for example by Lee [10].

The discrete ordinate method is also called the S_N-approximation, where N denotes the order of the quadrature rule. In one dimension, the order of the quadrature is the same as the number of direction and weights used for the quadrature. In two and three direction, the number of directions is larger than the order of the quadrature as shown in Table 3.1.

Dimensions	Directions
One	N
Two	$\frac{1}{2}N^2 + N$
Three	$N^2 + 2N$

Table 3.1: Number of directions M used by quadratures of order N.

3.2 Method of spherical harmonics and other moment based methods

The method of spherical harmonics, or the P_N-approximation, transforms the equation of radiative transfer into a system of infinite number of partial differential equations independent of direction. Taking only a finite number of equations and approximating the variables coupled with the removed

equations, we obtain an approximate solution of (3.1), the radiative transfer equation. Since we choose an arbitrarily large number of equations, we have an arbitrarily high order accuracy. The method of spherical harmonics was developed by Jeans [7]. Kourganoff [9] applied the method to radiative transfer. The method of spherical harmonics was applied to neutron transport problems by Davison [4] and Murray [14].

First we shall derive the popular P_1-approximation, as the derivation is substantially easier than for the general method. Then we shall describe the diffusion method, which approximates the P_1-approximation scheme with a diffusion equation. At the end of the section, we will discuss the general idea of the P_N-approximation.

3.2.1 P_1-approximation

The P_1-approximation of the equation (3.1), the radiative transfer equation, can be derived by taking the zeroth and first moment of (3.1) and decoupling them from higher moments of (3.1). The decoupling is achieved by assuming that the radiance vary linearly in direction.

It is very often the case that the desired quantity is irradiance E. Instead of indirectly calculating E by first solving (3.1) for I, we can manipulate the radiative transport equation to obtain an equation with E as the unknown function. Integrating (3.1) over the solid angle of 4π yields

$$\frac{1}{c}\frac{\partial E}{\partial t} + \nabla \cdot \mathbf{F} = 4\pi\sigma_{\mathrm{a}} B - (\sigma_{\mathrm{a}} + \sigma_{\mathrm{s}})E + \frac{\sigma_{\mathrm{s}}}{4\pi}\int_{4\pi}\int_{4\pi} \Psi(\mathbf{s}', \mathbf{s})\; d\Omega\; I(\mathbf{r}, \mathbf{s}', t)\; d\Omega'.$$

The condition (2.7) stays that $\int_{4\pi} \Psi(\mathbf{s}', \mathbf{s})\; d\Omega = 4\pi$, thus the equation above simplifies to

$$\frac{1}{c}\frac{\partial E}{\partial t} + \nabla \cdot \mathbf{F} = \sigma_{\mathrm{a}}(4\pi B - E), \tag{3.10}$$

where in-scattering and out-scattering cancel each other out. Let us realise that this equation is the zeroth moment of the equation (3.1). The equation (3.10) has a new unknown, radiative flux $\mathbf{F}$ defined by (3.5). We obtain an equation for $\mathbf{F}$ by taking the first moment of the equation (3.1) (multiplying the equation by s and integrating it over all directions), i.e.

$$\frac{1}{c}\frac{\partial \mathbf{F}}{\partial t} + \nabla \cdot \mathbb{P} = -(\sigma_{\mathrm{a}} + \sigma_{\mathrm{s}})\mathbf{F} + \frac{\sigma_{\mathrm{s}}}{4\pi}\int_{4\pi}\mathbf{s}\int_{4\pi} \Psi(\mathbf{s}', \mathbf{s}) I(\mathbf{r}, \mathbf{s}', t)\; d\Omega'\; d\Omega.$$

When we assume the scattering to be isotropic, that is $\Psi \equiv 1$, this equation simplifies further into the form

$$\frac{1}{c}\frac{\partial \mathbf{F}}{\partial t} + \nabla \cdot \mathbb{P} = -(\sigma_\mathrm{a} + \sigma_\mathrm{s})\mathbf{F}. \tag{3.11}$$

Here, we have employed the fact that the first moment $\int_{4\pi} \mathbf{s}\, d\Omega$ is equal to zero, see (3.3). This equation again contains a new unknown, the radiation pressure tensor $\mathbb{P}$ as defined by (3.6). We could continue this procedure and take higher and higher moments of (3.1), but each equation will always be coupled to the next higher moment of (3.1).

The idea of P_1-approximation is to approximate the tensor $\mathbb{P}$ in order to decouple the system from moments of (3.1) higher than one. To this end, we assume that the radiance varies linearly in direction, that is

$$I = a(\mathbf{r}) + \mathbf{b}(\mathbf{r}) \cdot \mathbf{s}. \tag{3.12}$$

Radiance and the radiative flux consequently satisfy

$$\begin{aligned} E &= \int_{4\pi} I \; d\Omega = a(\mathbf{r}) \int_{4\pi} d\Omega + \mathbf{b}(\mathbf{r}) \int_{4\pi} \mathbf{s} \; d\Omega = 4\pi a(\mathbf{r}), \\ \mathbf{F} &= \int_{4\pi} \mathbf{s} \; I \; d\Omega = a(\mathbf{r}) \int_{4\pi} \mathbf{s} \; d\Omega + \mathbf{b}(\mathbf{r}) \int_{4\pi} \mathbf{s} \otimes \mathbf{s} \; d\Omega = \frac{4\pi}{3}\mathbf{b}(\mathbf{r})\mathbb{I}, \end{aligned}$$

where we use the momentum values (3.2), (3.3) and (3.4). Replacing the functions a and $\mathbf{b}$ in (3.12) yields

$$I = \frac{1}{4\pi}E + \frac{3}{4\pi}\mathbf{s} \cdot \mathbf{F}.$$

We plug this particular form of radiance into the radiation pressure tensor and thereby derive

$$\mathbb{P} = \int_{4\pi} (\mathbf{s} \otimes \mathbf{s}) I \; d\Omega = \frac{1}{4\pi}E \int_{4\pi} \mathbf{s} \otimes \mathbf{s} \; d\Omega + \frac{3}{4\pi}\mathbf{F} \int_{4\pi} \mathbf{s} \; d\Omega = \frac{1}{3}E\mathbb{I}.$$

Plugging the approximation of the radiation pressure tensor into (3.11) and leaving (3.10) unchanged we arrive to a system of two equations and two unknowns independent of direction, namely

$$\frac{1}{c}\frac{\partial E}{\partial t} + \nabla \cdot \mathbf{F} = \sigma_\mathrm{a}(4\pi B - E), \tag{3.13}$$

$$\frac{1}{c}\frac{\partial \mathbf{F}}{\partial t} + \frac{1}{3}\nabla E = -(\sigma_\mathrm{a} + \sigma_\mathrm{s})\mathbf{F}. \tag{3.14}$$

This is called the P_1-approximation. An implication of the P_1-approximation is that there can be more energy moving, than the amount of energy that there actually is, since the magnitude of the flux $\mathbf{F}$ is not bounded by irradiance E. This conflict with reality is a substantial source of problems for the P_1-method.

3.2.2 Diffusion approximation

The diffusion method is based on the idea to approximate the system of equations (3.13) and (3.14) by a diffusion equation. We shall assume that the flux $\mathbf{F}$ varies slowly with time in comparison to spatial gradient, that is

$$\frac{1}{c}\frac{\partial \mathbf{F}}{\partial t} \ll \nabla E.$$

Using this assumption in (3.14) we obtain Flick's low

$$\mathbf{F} = -\frac{1}{3(\sigma_\mathrm{a} + \sigma_\mathrm{s})}\nabla E.$$

Plugging Flick's low into (3.13) gives us the diffusion equation

$$\frac{1}{c}\frac{\partial E}{\partial t} + \nabla \cdot D\nabla E = \sigma_\mathrm{a}(4\pi B - E), \tag{3.15}$$

with the diffusion coefficient $D = 1/3(\sigma_\mathrm{a} + \sigma_\mathrm{s})$.

The diffusion approximation makes substantial changes in the nature of the equation. The equation of radiative transfer or (3.1) is a hyperbolic partial differential equation, therefore describes particles traveling at a finite speed. The diffusion equation (3.15) is parabolic, which means that any change in the solution at a given place and time effect solution at all other places after an arbitrarily small instant. This is due to ignoring the time derivative in (3.14).

3.2.3 P_N-approximation

The derivation of *the P_N-approximation* is similar to the procedure we did in Section 3.2.1 to get the P_1-approximation of (3.1), the equation of radiative transfer. The difference is that instead of taking only the zeroth and first moments of (3.1) we can take as many moments as we need for an accurate solution. Moreover, instead of taking moments of (3.1) with respect to $\mathbf{s}$, we take the moments with respect to functions of $\mathbf{s}$, namely the spherical

harmonic functions. That is why this method is also called *the method of spherical harmonics*. We define *the spherical harmonic functions* as

$$Y_l^m(\mathbf{s}) = (-1)^{\frac{m+|m|}{2}} \left[\frac{(l-|m|)!}{(l+|m|)!}\right]^{\frac{1}{2}} e^{im\psi} P_l^{|m|}(\cos\theta),$$

where θ and ψ are respectively the polar and azimuthal angles of the vector $\mathbf{s}$ and P_l^m are associated Legendre polynomials. The spherical harmonics have the advantage of being orthogonal to one another, which is due to the use of Legendre polynomials.

We will explain only the general idea of how the method of spherical harmonics is derived for (3.1), the equation of heat transfer, as a detailed derivation is highly complicated. A thorough derivation of P_N-method in the tree-dimensional Cartesian coordinate system has been preformed by Cheng [3]. The extension to general coordinate systems has been given by Ou and Liou [15].

First of all, we need to expand the scattering phase function into series of Legendre polynomials. Now, multiplying (3.1) by each Y_l^m and integrating over all directions, we get infinitely many coupled equations, unknowns of which are moments of I with respect to Y_l^m. We denote the moment of I with respect to Y_l^m as

$$I_l^m(\mathbf{r},t) = \int_{4\pi} Y_l^m(\mathbf{s}) I(\mathbf{r},\mathbf{s},t)\, d\Omega. \tag{3.16}$$

Since $Y_0^0 = 1$ we have that $I_0^0 = E$. Each moment I_l^m is coupled to six other moments, namely all $I_{l'}^{m'}$, with $l' = l \pm 1$ and $m' = m + \{-1, 0, 1\}$. We can now express the radiance I in terms of generalised two-dimensional Fourier series

$$I(\mathbf{r},\mathbf{s},t) = \sum_{l=0}^{\infty} \sum_{m=-l}^{l} I_l^m(\mathbf{r},t) Y_l^m(\mathbf{s}). \tag{3.17}$$

To get a finite number of equations with a finite number of unknowns I_l^m, we choose an approximation order N and assume that $I_l^m = 0$ for $l > N$. In other words, we truncate the Fourier series (3.17). The resulting system can be written as follows (see [12]):

$$\frac{1}{c}\frac{\partial \mathbf{E}}{\partial t} + \mathbb{A}_x \frac{\partial \mathbf{E}}{\partial x} + \mathbb{A}_y \frac{\partial \mathbf{E}}{\partial y} + \mathbb{A}_z \frac{\partial \mathbf{E}}{\partial z} = \mathbf{S} - (\sigma_\mathrm{a} + \sigma_\mathrm{s})\mathbf{E}, \tag{3.18}$$

where $\mathbf{E}$ is a vector of moments E_l^m, $\mathbf{S}$ is the source vector containing the in-scattering and emission terms and $\mathbb{A}_x$, $\mathbb{A}_y$ and $\mathbb{A}_z$ are matrices that prescribe how the moments E_l^m are coupled.

3.3 Numerical defects

In this section we shall discuss unphysical numerical defects we might encounter when solving the equation of radiative transfer approximately. Typical drawbacks of approximation methods that are based on discretisation of variables are false scattering and the ray effect, which are respectively cause by spatial and directional discretisation. We can therefore expect discrete ordinate method to suffer exactly from these defects. The wave effect on the other hand is due to truncating the Fourier series in the method of spherical harmonics.

3.3.1 False scattering

False scattering (for different types of equations also called numerical diffusion) is a defect which arises from spatial discretisation. Although spatial discretisation is not of our concern in this chapter, we discuss it, because the effect results in additional unphysical scattering, which is a directional phenomenon.

In reality, when a single beam of electromagnetic radiation penetrates through a non-scattering medium, it travels in a straight line until it gets absorbed or reflected. When numerically computing this process, the beam widens, which means that part of the radiation was slightly redirected from the initial direction of the beam. This is due to the way we compute the numerical flux on the elements of the spatial partition, instead of calculating the real physical flux.

Therefore, we may observe scattering during numerical experiments in a non-scattering medium. In case of scattering medium, we then observe additional unphysical scattering. This is the reason why this effect is called false scattering. In case of other types of equations, the same effect appears as a different phenomenon, for instance diffusion.

When we employ the discrete ordinate method to solve the equation of radiative transfer, we need to solve the system (3.9) by standard methods, which typically discretise space. Hence, when applying discrete ordinates method, we must take false scattering into account.

Note that false scattering is a typical phenomenon that occurs due to low order discretisation in space. Higher order methods suffer from other defects, for instance from the phase error. We do not cover this phenomenon, as we will apply finite volume method, order of which is one. For more information about the phase error see [11].

3.3.2 Ray effect

The ray effect is caused by the directional discretisation, which allows the particles to travel only in selected directions. This effect is typical for discrete ordinate method.

The ray effect becomes apparent, for instance, when we are further from a high emission source of particles. Suppose we have a spatial partition. Event though in reality, the source emits radiation to all directions equally, the ray effect may cause the rays to become so far apart that there are two adjacent elements of the partition, one with no radiance at all and the other with plenty of radiance coming from the source. This results in large spatial oscillations in irradiance E. This effect can be reduced either by increasing the number of directions or by taking a sparser spatial partition with larger elements.

Hence, when refining the spatial partition, we need to increase the number of considered directions accordingly, in order to prevent the ray effect to become significant.

3.3.3 Wave effect

The wave effect is a defect of the method of spherical harmonics. In vacuum, for the zero right-hand side, the system (3.18) becomes a wave equation, which allows negative irradiance. This unphysical phenomenon may occur even in regions where a participating medium is present.

Chapter 4

Finite volume method for the transport equation

In the previous chapter, we summarised a few numerical method that discretise only direction. The main target of this thesis is to derive and apply the finite volume method for the equation of radiative transfer in both two-dimensional spatial and one-dimensional directional variables.

In this chapter, we will introduce the finite volume method for the spatial discretisation. The directional approximation will be dealt with in the following chapter. As the equation of radiative transfer is first order linear partial differential equation in space, we will derive the method for a two-dimensional transport equation, namely

$$\mathbf{u}_t + \mathbf{p}_x(\mathbf{u}) + \mathbf{q}_y(\mathbf{u}) = \mathbf{f}, \tag{4.1}$$

which is of course also first order and linear, so we can conveniently apply the acquired knowledge for the equation of radiative transfer in the following chapter. Here, $\mathbf{u}$ is the unknown function, $\mathbf{p}$ and $\mathbf{q}$ are given physical fluxes in the direction x and y, respectively, and $\mathbf{f}$ is a given source function. The finite volume method was also described by Leveque [11] and in many other standard textbooks.

4.1 Notation

We first introduce some notation regarding especially the spatial partition. Let Ω be a domain in $\mathbb{R}^2$ and Ω_h an approximation of Ω with a piecewise linear boundary. Let $\mathcal{T}_h = \{\Omega_i\}_{i\in J}$, $J = \{0, 1, \ldots, m\}$, be a triangle partition of Ω_h. In other words, Ω_i, $i \in J$, are triangles with mutually disjoint interiors

such that

$$\overline{\Omega}_h = \bigcup_{i \in J} \Omega_i.$$

The length of the longest edge in $\mathcal{T}_h$ will be denoted as h. We say that Ω_i is a neighbour of Ω_j, if the intersection $\ell_{ij} = \Omega_i \cap \Omega_j$ is a line segment and we denote the set of indexes of neighbours of Ω_i by N_i, i.e. $N_i = \{j \in J : \Omega_i \cap \Omega_j \text{ is a line segment}\}$. Let $\{\ell^b_{-1}, \ell^b_{-2}, \ldots, \ell^b_{-k}\}$ be the set of all the line segments of $\partial\Omega_h$ such that each line segment is a face of a triangle in $\mathcal{T}_h$ and let us denote $J^b = \{-1, -2, \ldots, -k\}$. Note that $J \cap J^b = \emptyset$ and

$$\partial\Omega_h = \bigcup_{j \in J^b} \ell^b_j.$$

Let $i \in J$. We use the following notation

$$N^b_i = \{j \in J^b : \ell^b_j \subset \partial\Omega_i\}.$$

For $i \in J$ and $j \in N^b_i$ we set $\ell_{ij} = \ell^b_j$. Hence, ℓ_{ij} is either a common face between Ω_i and Ω_j (if $j \in J$), or a face of Ω_i on $\partial\Omega_h$ (if $j \in J^b$). The length of ℓ_{ij} is denoted by $|\ell_{ij}|$ and its unit outer normal by $\mathbf{n}_{ij} = (n^x_{ij}, n^y_{ij})$. Furthermore, the area of Ω_i is $|\Omega_i|$.

Let $0 = t_0 < t_1 < \ldots < t_{M_t} = T$ be a partition of the interval $[0, T]$ where $M_t \in \mathbb{N}$ and $T > 0$. We call $\tau_k = [t_k, t_{k+1}]$ a *time step* and $|\tau_k|$ is its length.

4.2 Numerical flux

Before we start with the derivation of the finite volume method, we shall introduce the numerical flux, which we will use later. We consider the physical fluxes $\mathbf{p}$ in the direction x and $\mathbf{q}$ in the direction y from (4.1). If $\mathbb{J}_\mathbf{p}$ and $\mathbb{J}_\mathbf{q}$ are respectively the Jacobi matrices of $\mathbf{p}$ and $\mathbf{q}$, then

$$\mathcal{P}(\mathbf{u}, \mathbf{n}) = \mathbf{p}(\mathbf{u})n^x + \mathbf{q}(\mathbf{u})n^y, \tag{4.2}$$

is the physical flux in the direction $\mathbf{n}$ and its Jacobi matrix is

$$\mathbb{J}_\mathcal{P}(\mathbf{u}, \mathbf{n}) = \mathbb{J}_\mathbf{p}(\mathbf{u})n^x + \mathbb{J}_\mathbf{q}(\mathbf{u})n^y.$$

The physical flux $\mathcal{P}(\mathbf{u}, \mathbf{n})$ is the amount of the considered substance passing trough a unit line segment perpendicular to $\mathbf{n}$ per unit time. In this section, we shall define numerical flux, which is the same quantity as the physical flux in the discrete scheme.

Before we diagonalise the matrix $\mathbb{J}_{\mathcal{P}}$, let us define what a diagonalisable matrix means. A square matrix $\mathbb{M}$ is called *diagonalisable* if it is similar to a diagonal matrix, say $\mathbb{D}$, i.e. if there exists a matrix $\mathbb{V}$ such that $\mathbb{V}^{-1}\mathbb{M}\mathbb{V} = \mathbb{D}$. The characterisation of diagonalisable matrices is the following: An $n \times n$ matrix $\mathbb{M}$ is diagonalisable if and only if it has n linearly independent eigenvectors. Suppose that this is the case and let $\mathbf{v}_1, \mathbf{v}_2, \ldots, \mathbf{v}_n$ be eigenvectors corresponding respectively to the eigenvalues $\lambda_1, \lambda_2, \ldots, \lambda_n$ of $\mathbb{M}$. Then for the matrix $\mathbb{V} = (\mathbf{v}_1, \mathbf{v}_2, \ldots, \mathbf{v}_n)$ there exists its inverse $\mathbb{V}^{-1}$ and $\mathbb{V}^{-1}\mathbb{M}\mathbb{V} = \mathbb{D}$ where $\mathbb{D} = \mathrm{diag}(\lambda_1, \lambda_2, \ldots, \lambda_n)$. Note that we can comfortably use Matlab built-in routine *eig* in order to diagonalise matrices.

Let us suppose that $\mathbb{J}_{\mathcal{P}}(\mathbf{u}, \mathbf{n})$ is diagonalisable matrix with real eigenvalues. Then there is a matrix $\mathbb{V}$ such that

$$\mathbb{J}_{\mathcal{P}} = \mathbb{V}^{-1}\mathbb{D}\mathbb{V}, \quad \mathbb{D} = \mathrm{diag}(\lambda_1, \lambda_2, \ldots, \lambda_n).$$

We separate $\mathbb{J}_{\mathcal{P}}$ and $\mathbb{D}$ into the positive and the negative parts as follows

$$\begin{aligned} \mathbb{J}_{\mathcal{P}}^{\pm} &= \mathbb{V}^{-1}\mathbb{D}^{\pm}\mathbb{V}, \\ \mathbb{D}^{\pm} &= \mathrm{diag}(\lambda_1^{\pm}, \lambda_2^{\pm}, \ldots, \lambda_n^{\pm}), \end{aligned} \tag{4.3}$$

with

$$\begin{aligned} \lambda_i^{+} &= \max(0, \lambda_i), \\ \lambda_i^{-} &= \min(0, \lambda_i). \end{aligned}$$

Clearly

$$\mathbb{J}_{\mathcal{P}} = \mathbb{J}_{\mathcal{P}}^{+} + \mathbb{J}_{\mathcal{P}}^{-}.$$

The absolute value of $\mathbb{J}_{\mathcal{P}}$ will be understood as

$$|\mathbb{J}_{\mathcal{P}}| = \mathbb{V}^{-1}|\mathbb{D}|\mathbb{V}, \quad |\mathbb{D}| = \mathrm{diag}(|\lambda_1|, |\lambda_2|, \ldots, |\lambda_n|).$$

4.2.1 Examples of numerical fluxes

We will list a few fluxes that are widely used (see also [5], Section 4.4.4).

(a) Steger-Warming numerical flux:

$$\mathcal{H}(\mathbf{u}, \mathbf{v}, \mathbf{n}) = \mathbb{J}_{\mathcal{P}}^{+}(\mathbf{u}, \mathbf{n})\mathbf{u} + \mathbb{J}_{\mathcal{P}}^{-}(\mathbf{v}, \mathbf{n})\mathbf{v}. \tag{4.4}$$

(b) Vijayasundaram numerical flux:

$$\mathcal{H}(\mathbf{u}, \mathbf{v}, \mathbf{n}) = \mathbb{J}_{\mathcal{P}}^{+}\left(\frac{\mathbf{u}+\mathbf{v}}{2}, \mathbf{n}\right)\mathbf{u} + \mathbb{J}_{\mathcal{P}}^{-}\left(\frac{\mathbf{u}+\mathbf{v}}{2}, \mathbf{n}\right)\mathbf{v}.$$

(c) Lax-Friedrichs numerical flux:

$$\mathcal{H}(\mathbf{u},\mathbf{v},\mathbf{n}) = \frac{1}{2}\left[\mathcal{P}(\mathbf{u},\mathbf{n}) + \mathcal{P}(\mathbf{v},\mathbf{n}) - \frac{1}{c}(\mathbf{v}-\mathbf{u})\right],$$

where $c > 0$ is suitably chosen and independent of $\mathbf{u}$ and $\mathbf{v}$.

(d) Van Leer numerical flux:

$$\mathcal{H}(\mathbf{u},\mathbf{v},\mathbf{n}) = \frac{1}{2}\left[\mathcal{P}(\mathbf{u},\mathbf{n}) + \mathcal{P}(\mathbf{v},\mathbf{n}) - \left|\mathbb{J}_{\mathcal{P}}\left(\frac{\mathbf{u}+\mathbf{v}}{2},\mathbf{n}\right)\right|(\mathbf{v}-\mathbf{u})\right]. \tag{4.5}$$

4.2.2 Properties of the numerical flux

The numerical flux is essential for the correct functioning of the whole algorithm. Often the schemes vary mainly by the choice of the numerical flux. Let D be the domain of definition of $\mathbf{p}$ and $\mathbf{q}$ and $\mathcal{S}_1$ the unit sphere. We must be careful for our chosen numerical flux to satisfy the following three conditions (see also [5], Section 4.4.3):

(1) Continuity:

$$\mathcal{H} \text{ is defined and continuous on } D \times D \times \mathcal{S}_1.$$

(2) Consistency:

$$\mathcal{H}(\mathbf{u},\mathbf{u},\mathbf{n}) = \mathcal{P}(\mathbf{u},\mathbf{n}).$$

(3) Conservativity:

$$\mathcal{H}(\mathbf{u},\mathbf{v},\mathbf{n}) = -\mathcal{H}(\mathbf{u},\mathbf{v},-\mathbf{n}).$$

Note that these conditions are not implicitly true or false for a given numerical flux. Their satisfaction also depends on the given equation, more precisely on the properties of the physical fluxes $\mathbf{p}$ and $\mathbf{q}$.

4.3 Derivation of a finite volume scheme

We consider the following problem for the equation (4.1):
Find $\mathbf{u} : \Omega \times [0,T] \to \mathbb{R}^d$, $d \in \mathbb{N}$, such that

$$\mathbf{u}_t + \mathbf{p}_x(\mathbf{u}) + \mathbf{q}_y(\mathbf{u}) = \mathbf{f}(x,y,t) \qquad \text{in } \Omega \times (0,T], \tag{4.6}$$

which is subject to the initial condition

$$\mathbf{u} = \mathbf{u}_0(x, y) \qquad \text{in } \Omega \times \{0\}, \tag{4.7}$$

and the boundary condition

$$\mathbf{u} = \mathbf{b}(x, y, t), \tag{4.8}$$

that needs to be satisfied for each equation of the system on its inlet part of the boundary. Here the boundary function $\mathbf{b}$, initial function $\mathbf{u}_0$, source function $\mathbf{f}$ and physical fluxes $\mathbf{p}$ and $\mathbf{q}$ are given functions with d components.

4.3.1 Temporal discretisation

At first, we will discretise the time variable by the explicit Euler method. Integrating the equations (4.6) over $\tau_k = [t_k, t_{k+1}]$ yields

$$\mathbf{u}(\mathbf{r}, t_{k+1}) - \mathbf{u}(\mathbf{r}, t_k) + \int_{\tau_k} \Big[\mathbf{p}_x(\mathbf{u}) + \mathbf{q}_y(\mathbf{u})\Big]\ dt = \int_{\tau_k} \mathbf{f}(\mathbf{r}, t)\ dt$$

where $\mathbf{r} = (x, y)$ is the location vector. Following the Euler method, we approximate the integral on the left-hand side by the left endpoint rule and join the equations (4.7) and (4.8) to obtain the semi-discrete scheme:

$$\mathbf{u}^{k+1} = \mathbf{u}^k - |\tau_k|\Big[\mathbf{p}_x(\mathbf{u}^k) + \mathbf{q}_y(\mathbf{u}^k)\Big] + \int_{\tau_k} \mathbf{f}(\mathbf{r}, t)\ dt \qquad \text{in } \Omega_i, \tag{4.9}$$

which is subject to the initial and boundary conditions

$$\begin{aligned} \mathbf{u}^0(\mathbf{r}) &= \mathbf{u}_0(\mathbf{r}) && \mathbf{r} \in \Omega_i, \\ \mathbf{u}^k(\mathbf{r}_b) &= \mathbf{b}(\mathbf{r}_b, t_k) && \mathbf{r}_b \in \partial\Omega_i. \end{aligned} \tag{4.10}$$

The boundary condition is again prescribed for each of the d equations only on their inlet part of the boundary. The function $\mathbf{u}^k$ is an approximation of the exact solution $\mathbf{u}$ at time t_k, that means

$$\mathbf{u}^k(\mathbf{r}) \approx \mathbf{u}(\mathbf{r}, t_k).$$

4.3.2 Spatial discretisation

Now, we will move on to the finite volume disretisation of the spatial variable. To this end, we integrate the equations (4.9) and (4.10) over a triangle Ω_i,

$i \in J$,

$$\int_{\Omega_i} \mathbf{u}^{k+1}\ d\mathbf{r} = \int_{\Omega_i} \mathbf{u}^k\ d\mathbf{r} - |\tau_k| \int_{\Omega_i} \Big[\mathbf{p}_x\big(\mathbf{u}^k\big) + \mathbf{q}_y\big(\mathbf{u}^k\big)\Big]\ d\mathbf{r} + |\Omega_i|\mathbf{F}_i^k, \tag{4.11}$$

$$\int_{\Omega_i} \mathbf{u}^0\ d\mathbf{r} = \int_{\Omega_i} \mathbf{u}_0\ d\mathbf{r}, \tag{4.12}$$

where

$$\mathbf{F}_i^k = \frac{1}{|\Omega_i|} \int_{\tau_k} \int_{\Omega_i} \mathbf{f}(\mathbf{r}, t)\ d\mathbf{r}\ dt. \tag{4.13}$$

We rearrange the third term in the equation (4.11) as follows

$$\begin{aligned}\int_{\Omega_i} \Big[\mathbf{p}_x\big(\mathbf{u}^k\big) + \mathbf{q}_y\big(\mathbf{u}^k\big)\Big]\ d\mathbf{r} &= \int_{\partial\Omega_i} \Big[\mathbf{p}\big(\mathbf{u}^k\big)n^x + \mathbf{q}\big(\mathbf{u}^k\big)n^y\Big]\ d\ell \\ &= \int_{\partial\Omega_i} \mathcal{P}\big(\mathbf{u}^k, \mathbf{n}\big)\ d\ell = \sum_{j \in N_i \cup N_i^b} \int_{\ell_{ij}} \mathcal{P}\big(\mathbf{u}^k, \mathbf{n}_{ij}\big)\ d\ell,\end{aligned}$$

with $d\ell = |d\mathbf{r}| = \sqrt{(dx)^2 - (dy)^2}$ and the outer normal $\mathbf{n}(\mathbf{r}) = (n^x(\mathbf{r}), n^y(\mathbf{r}))$ of $\partial\Omega_i$. Recall that $\mathbf{n}_{ij}$ is the outer normal of ℓ_{ij}. The first equality follows from Green's theorem. The integrand in the second term is nothing else than the physical flux $\mathcal{P}$ in the direction $\mathbf{n}$, see (4.2). Finally, instead of integrating over the circumference of Ω_i, we can integrate over each of the three faces of the triangle separately, hence the third equality. Plugging the acquired expression into the equation (4.11) and dividing it by the area $|\Omega_i|$ we obtain

$$\frac{1}{|\Omega_i|} \int_{\Omega_i} \mathbf{u}^{k+1}\ d\mathbf{r} = \frac{1}{|\Omega_i|} \int_{\Omega_i} \mathbf{u}^k\ d\mathbf{r} - \frac{|\tau_k|}{|\Omega_i|} \sum_{j \in N_i \cup N_i^b} \int_{\ell_{ij}} \mathcal{P}\big(\mathbf{u}^k, \mathbf{n}_{ij}\big)\ d\ell + \mathbf{F}_i^k, \tag{4.14}$$

for all $i \in J$. We denote the approximation of the integral average of $\mathbf{u}^k$ over $|\Omega_i|$ as

$$\mathbf{U}_i^k \approx \frac{1}{|\Omega_i|} \int_{\Omega_i} \mathbf{u}^k\ d\mathbf{r}.$$

Now, we will focus on the approximation of $\int \mathcal{P}\big(\mathbf{u}^k, \mathbf{n}_{ij}\big)\ d\ell$. At each time step k, we approximate $\mathbf{u}^k$ by a piecewise constant function $\mathbf{u}_h^k$ such that $\mathbf{u}_h^k = \mathbf{U}_i^k$ in the interior of Ω_i, $i \in J$. If $j \in J$ (i.e. ℓ_{ij} is not a part

of boundary $\partial\Omega_h$), then the function $\mathbf{u}_h^k$ has the value $\mathbf{U}_i^k$ on the left hand side and $\mathbf{U}_j^k$ on the right hand side of the line segment ℓ_{ij}. We plug the two integral averages $\mathbf{U}_i^k$ and $\mathbf{U}_j^k$ that surround ℓ_{ij} into the numerical flux $\mathcal{H}$ (see section 4.2)

$$\mathcal{H}\big(\mathbf{U}_i^k, \mathbf{U}_j^k, \mathbf{n}_{ij}\big) \approx \frac{1}{|\ell_{ij}|} \int\limits_{\ell_{ij}} \mathcal{P}\big(\mathbf{u}^k, \mathbf{n}_{ij}\big)\ d\ell \qquad \text{for } i, j \in J.$$

In the case where $j \in J^b$ (i.e. $\ell_{ij} = \ell_j^b$ is a part of the boundary $\partial\Omega_h$), $\mathbf{u}_h^k$ has again the value $\mathbf{U}_i^k$ on the left hand side of ℓ_{ij}. As a value on the right hand side, we will use the integral average of the boundary function $\mathbf{b}$ over ℓ_{ij} and plug that into the numerical flux $\mathcal{H}$

$$\mathcal{H}\left(\mathbf{U}_i^k, \frac{1}{|\ell_{ij}|} \int\limits_{\ell_{ij}} \mathbf{b}(\mathbf{r}, t_k)\right) \approx \frac{1}{|\ell_{ij}|} \int\limits_{\ell_{ij}} \mathcal{P}\big(\mathbf{u}^k, \mathbf{n}_{ij}\big)\ d\ell \qquad \text{for } i \in J,\ j \in J^b.$$

We will unify the notation of approximation of integral averages of $\mathbf{u}^k$ as follows:

$$\mathbf{U}_j^k \approx \begin{cases} \dfrac{1}{|\Omega_j|} \displaystyle\int\limits_{\Omega_j} \mathbf{u}^k\ d\mathbf{r} & \text{for } j \in J, \\ \dfrac{1}{|\ell_j^b|} \displaystyle\int\limits_{\ell_j^b} \mathbf{b}(\mathbf{r}, t_k)\ d\mathbf{r} & \text{for } j \in J^b. \end{cases} \tag{4.15}$$

Then we can write

$$\mathcal{H}\big(\mathbf{U}_i^k, \mathbf{U}_j^k, \mathbf{n}_{ij}\big) \approx \frac{1}{|\ell_{ij}|} \int\limits_{\ell_{ij}} \mathcal{P}\big(\mathbf{u}^k, \mathbf{n}_{ij}\big)\ d\ell \qquad \text{for } i \in J,\ j \in J \cup J^b. \tag{4.16}$$

Plugging approximations (4.15) and (4.16) into equations (4.12) and (4.14) we derive the fully-discrete scheme

$$\mathbf{U}_i^k = \frac{1}{|\ell_i^b|} \int\limits_{\ell_i^b} \mathbf{b}(\mathbf{r}, t_k)\ d\mathbf{r} \qquad i \in J^b, \tag{4.17}$$

$$\mathbf{U}_i^0 = \frac{1}{|\Omega_i|} \int\limits_{\Omega_i} \mathbf{u}_0\ d\mathbf{r}, \qquad i \in J, \tag{4.18}$$

$$\mathbf{U}_i^{k+1} = \mathbf{U}_i^k - \frac{|\tau_k|}{|\Omega_i|} \sum_{j \in N_i \cup N_i^b} |\ell_{ij}| \mathcal{H}\big(\mathbf{U}_i^k, \mathbf{U}_j^k, \mathbf{n}_{ij}\big) + \mathbf{F}_i^k \qquad i \in J. \tag{4.19}$$

Let us recall that $N_i \subset J$, $N_i^b \subset J^b$ and $J \cap J^b = \emptyset$. This completes our main target of this chapter, as the three equations above prescribe the finite volume method for the transfer equation (4.1). The only work left is to approximate the integrals in (4.13), (4.17) and (4.18).

4.3.3 Approximation of integrals

Since the values of $\mathbf{U}_i^k$ are given recursively by the equation (4.19) for $i \in J$ and $k \geq 1$, we need to evaluate $\mathbf{U}_i^0$ (the equation (4.18)) and $\mathbf{U}_i^k$ for $i \in J_b$ (the equation (4.17)). While we can employ numerical quadratures of an arbitrary order, we will describe only the one-point rules here.

In order to approximate the integral in (4.18), we take the value of $\mathbf{u}_0$ at the centroid of Ω_i. If $\mathbf{a} = (x_a, y_a)$, $\mathbf{b} = (x_b, y_b)$, $\mathbf{c} = (x_c, y_c)$ are vertexes of Ω_i, then

$$\mathbf{r}_i = \frac{\mathbf{a}+\mathbf{b}+\mathbf{c}}{3} = \frac{1}{3}\left(x_a + x_b + x_c,\ y_a + y_b + y_c\right), \tag{4.20}$$

is the centroid of Ω_i and

$$|\Omega_i| \cdot \mathbf{u}_0(\mathbf{r}_i) \approx \int_{\Omega_i} \mathbf{u}_0(\mathbf{r})\ d\mathbf{r}.$$

Therefore we set

$$\mathbf{U}_i^0 = \mathbf{u}_0(\mathbf{r}_i), \quad i \in J.$$

We approximate the integral in (4.17) by the midpoint rule

$$\mathbf{U}_j^k = \mathbf{b}(\mathbf{r}_j, t_k), \quad j \in J^b,$$

where $\mathbf{r}_j$ is the center of the line segment ℓ_j^b.

It remains to evaluate the source term (4.13). We approximate the integral with respect to $\mathbf{r}$ by the value at the centroid of Ω_i times its area and the integral with respect to t by the left endpoint rule. Hence we have

$$\mathbf{F}_i^k = |\tau_k|\mathbf{f}(\mathbf{r}_i, t_k), \quad i \in J.$$

4.4 Courant-Friedrichs-Lewy condition

In two dimensions the Courant-Friedrichs-Lewy condition reads

$$\frac{|v^x||\tau_k|}{\Delta x} + \frac{|v^y||\tau_k|}{\Delta y} \leq 1.$$

Here Δx and Δy are lengths of the interval of the spatial partition and v^x and v^y are velocities by which the solution propagates in x and y direction, respectively. As we have the triangular partition, we do not explicitly have the lengths Δx and Δy. On the triangle Ω_i, we approximate the lengths by the diameter d_i of the incircle of Ω_i, i.e.

$$d_i \approx \Delta x \approx \Delta y.$$

This yields

$$\frac{|\tau_k|}{d_i}\big(|v^x| + |v^y|\big) \leq 1.$$

The absolute values of velocities v^x and v^y are lower or equal to the absolute value of maximum eigenvalues $\lambda^{\mathbf{p}}_{\max}\big(U_i^k\big)$ of $\mathbb{J}_{\mathbf{p}}\big(U_i^k\big)$ and $\lambda^{\mathbf{q}}_{\max}\big(U_i^k\big)$ of $\mathbb{J}_{\mathbf{q}}\big(U_i^k\big)$, respectively. Taking this into account the Courant-Friedrichs-Lewy condition becomes

$$|\tau_k| \leq \frac{d_i}{\big|\lambda^{\mathbf{p}}_{\max}\big(U_i^k\big)\big| + \big|\lambda^{\mathbf{q}}_{\max}\big(U_i^k\big)\big|}. \tag{4.21}$$

4.5 Test of convergence

We will test our derived scheme on a nonlinear scalar and a linear vector problems. Firstly, let us set the parameters for the solver. We use Matlab built-in routine *initmesh* to generate the partition $\mathcal{T}_h$ of Ω_h, with the maximum edge size h. At each time step t_k we choose the longest time step $|\tau_k|$ such that the Courant-Friedrichs-Lewy condition holds true for a given h.

Let $\mathbf{u}_h$ denote the approximate solution generated by our solver and let the residuum at time t_k be

$$\mathrm{res}_k = \int_{\Omega_h} \big|\mathbf{u}_h(\mathbf{r}, t_k) - \mathbf{u}_h(\mathbf{r}, t_{k-1})\big|\, d\mathbf{r} = \sum_{i\in J} |\Omega_i|\big|\mathbf{U}_i^k - \mathbf{U}_i^{k-1}\big|, \tag{4.22}$$

for $k \geq 1$. We end the calculation when the residuum decreases below 10^{-4}. Let $K \in \mathbb{N}_0$ be the smallest number such that $\mathrm{res}_K < 10^{-4}$. We consider the approximate solution at time t_K to be at steady state. As a measure of accuracy of the approximate solution, we take the L_1-error at steady state, i.e.

$$\mathrm{err}_h = \sum_{i\in J} |\Omega_i|\big|\mathbf{u}(\mathbf{r}_i) - \mathbf{U}_i^K\big| \approx \int_{\Omega_h} \big|\mathbf{u}(\mathbf{r}) - \mathbf{u}_h(\mathbf{r}, t_K)\big|\, d\mathbf{r},$$

where $\mathbf{u}$ is the exact steady-state solution and $\mathbf{r}_i$ is the centroid (4.20) of Ω_i. The index h in err_h is the maximum edge size of the spatial partition $\mathcal{T}_h$. We define the convergence rate as follows

$$\mathrm{rate}_h = \log_2\left(\frac{\mathrm{err}_{2h}}{\mathrm{err}_h}\right). \tag{4.23}$$

Since we were using the first order approximation throughout the derivation of the finite volume scheme, we expect the convergence rate to be around one.

4.5.1 Exemplary computation for a nonlinear scalar equation

We consider the scalar analogy of the problem given by equations (4.6), (4.7), (4.8):

$$\begin{aligned} u_t + p_x(u) + q_y(u) &= f(x,y,t) && \text{in } \Omega \times (0,T), \\ u &= b(x,y,t) && \text{on } \partial\Omega \times (0,T), \\ u &= u_0(x,y) && \text{in } \Omega \times \{0\}, \end{aligned} \tag{4.24}$$

where f, p, q, b and u_0 are given scalar functions. Here we have the flux

$$\mathcal{P}(u,\mathbf{n}) = p(u)n^x + q(u)n^y,$$

which is a scalar. Thus, the Jacobi matrix $\mathbb{J}_{\mathcal{P}}$ also becomes scalar and, in this subsection, we will denote it by P, i.e.

$$\mathrm{P}(u,\mathbf{n}) = \frac{\partial \mathcal{P}(u,\mathbf{n})}{\partial u} = p'(u)n^x + q'(u)n^y.$$

We will be using the Van Leer flux (4.5):

$$\mathcal{H}(u,v,\mathbf{n}) = \frac{1}{2}\left[\mathcal{P}(u,\mathbf{n}) + \mathcal{P}(v,\mathbf{n}) - \left|\mathrm{P}\left(\frac{u+v}{2},\mathbf{n}\right)\right|(v-u)\right].$$

In order to test the scheme given by equations (4.17), (4.18) and (4.19), we need to choose f, p, q, b and u_0. Let $\Omega = \Omega_h = [0,1] \times [0,1]$ and let

$$\begin{aligned} u_0(x,y) &= \frac{1}{2}x^2 + \frac{1}{4}y, \\ p(u) &= \frac{1}{3}u^3, \\ q(u) &= \frac{1}{4}u^2 + \frac{1}{2}u. \end{aligned}$$

Consequently we have

$$\begin{aligned} p'(u) &= u^2, \\ q'(u) &= \frac{1}{2}(u+1). \end{aligned}$$

We take the stationary function

$$u(x,y) = \sin(\pi x) + 1 - e^{-\frac{\pi}{2}y},$$

to be the exact solution of (4.24). It follows that the source term takes the form

$$f(x,y) = \pi \cos^2(\pi x) - \frac{\pi}{4} e^{-\pi y} + \frac{1}{2},$$

and the boundary condition takes the form

$$\begin{aligned} u(x,0) &= \sin(\pi x) + 1, \\ u(x,1) &= \sin(\pi x) + 1 - e^{-\frac{\pi}{2}}, \\ u(0,y) &= u(1,y) = 1 - e^{-\frac{\pi}{2}y}. \end{aligned}$$

It is convenient to choose the time step to be the largest obeying (4.21):

$$|\tau_k| = \min_i \left(\frac{d_i}{\left|g'\left(U_i^k\right)\right| + \left|h'\left(U_i^k\right)\right|} \right),$$

where d_i is the indiameter of Ω_i.

Now, we pretend not to know the exact solution u of (4.24) and solve the problem by the finite volume solver for five different meshes with maximum edge size $h = 1/2,\ 1/4,\ 1/8,\ 1/16,\ 1/32$, thereby producing five approximate solutions u_h. The error of the approximate stationary solution $u_h(\cdot, t_K)$ is plotted in Figure 4.1 and tabulated in Table 4.1. The table also contains the number of time steps which needed to be taken to reach steady state along with the convergence rates. Let us note that the number of time steps $K = K_h$ depends on h. We emphasise that all the errors are taken at the last time step (at steady state) and so we need to run the whole algorithm for each of the five tabulated errors separately. We can see that the convergence rate is slightly lower than one, which means that the solver for this set of parameters converged somewhat slower than linearly.

h	K_h	err_h	rate_h
1/2	98	0.235	
1/4	125	0.135	0.796
1/8	146	0.0595	1.18
1/16	320	0.0325	0.871
1/32	656	0.0189	0.782

Table 4.1: The error, convergence rate and number of time steps at steady state of the scalar problem (4.24) for various values of h.

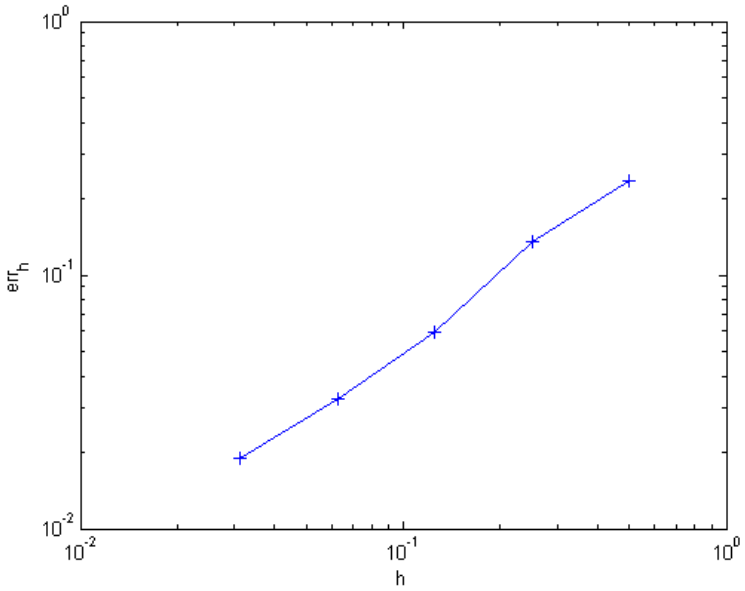

Figure 4.1: The error at steady state of the scalar problem (4.24) plotted for $h = 1/2,\ 1/4,\ 1/8,\ 1/16,\ 1/32$. The x and the y axes are proportional to $\log_{10} h$ and $\log_{10}(\mathrm{err}_h)$, respectively.

4.5.2 Exemplary computation for a linear vector equation

We consider the linear analogy of the problem given by equations (4.6), (4.7), (4.8) with

$$\mathbf{p}(\mathbf{u}) = \mathbb{A}\mathbf{u},$$
$$\mathbf{q}(\mathbf{u}) = \mathbb{B}\mathbf{u}.$$

Here $\mathbb{A}$, $\mathbb{B} \in \mathbb{R}^d$ are diagonalisable matrices. The flux becomes

$$\mathcal{P}(\mathbf{u}, \mathbf{n}) = \mathbb{A}\mathbf{u}\mathbf{n}^{\mathbf{x}} + \mathbb{B}\mathbf{u}\mathbf{n}^{\mathbf{y}},$$

and its Jacobi matrix

$$\mathbb{J}_{\mathcal{P}}(\mathbf{n}) = \mathbb{A}\mathbf{n}^{\mathbf{x}} + \mathbb{B}\mathbf{n}^{\mathbf{y}},$$

is independent of u. This results in the equivalence of Steger-Warming, Vijayasundaram, and Van Leer numerical fluxes. In the linear case, all of the three numerical fluxes can be written in the following form

$$\mathcal{H}(\mathbf{u}, \mathbf{v}, \mathbf{n}) = \mathbb{J}^{+}_{\mathcal{P}}(\mathbf{n})\mathbf{u} + \mathbb{J}^{-}_{\mathcal{P}}(\mathbf{n})\mathbf{v}.$$

For our experiment, we choose $\dim = 2$, $\Omega = \Omega_h = [0, 1] \times [0, 1]$ and

$$\mathbb{A} = \begin{pmatrix} 1 & 0.5 \\ 0.2 & 0.5 \end{pmatrix}, \qquad \mathbb{B} = \begin{pmatrix} 1 & 0.5 \\ 0.7 & 1.1 \end{pmatrix}.$$

Furthermore we choose the initial condition as

$$\mathbf{u}_0 \equiv \begin{pmatrix} 1 \\ 1 \end{pmatrix}.$$

We take

$$\mathbf{u}(x, y) = \begin{pmatrix} \sin(\pi x)\sin(\pi y) \\ 15(x - x^2)(y - y^2) \end{pmatrix}$$

to be the exact solution. We can now derive the source term by plugging the exact solution into (4.6). It is easy to see that we have the zero boundary condition $\mathbf{b} \equiv 0$. We choose the time step to be the largest obeying the condition (4.21):

$$|\tau| = \frac{\min_i d_i}{\left|\lambda^{\mathbb{A}}_{\max}\right| + \left|\lambda^{\mathbb{B}}_{\max}\right|}. \tag{4.25}$$

Here d_i is again the indiameter of Ω_i, $\lambda^{\mathbb{A}}_{\max}$ is the maximum eigenvalue of $\mathbb{A}$ and $\lambda^{\mathbb{B}}_{\max}$ is the maxim eigenvalue of $\mathbb{B}$. In the linear case, Courant-Friedrichs-Lewy condition does not depend on k, therefore there is no reason not to choose the mesh to be uniform with $|\tau| = |\tau_0| = |\tau_1| = \ldots$

Again, we proceed the algorithm for five partitions of Ω with $h = 1/2$, $1/4$, $1/8$, $1/16$, $1/32$. The error at steady state, the number of time steps needed to reach steady state and the convergence rate are shown in Table 4.2. The error is also plotted in Figure 4.2. Here, the acquired convergence rate confirm the suggested linear convergence by having its value close to one.

		first component		second component	
h	K_h	err_h^1	rate_h^1	err_h^2	rate_h^2
1/2	54	0.248		0.198	
1/4	89	0.135	0.883	0.119	0.74
1/8	152	0.0676	0.992	0.0718	0.725
1/16	317	0.0369	0.873	0.0398	0.852
1/32	568	0.0199	0.893	0.0206	0.951

Table 4.2: The error, convergence rate and number of time steps at steady state of the vector problem for various values of h. The upper indexes denote the component numbers.

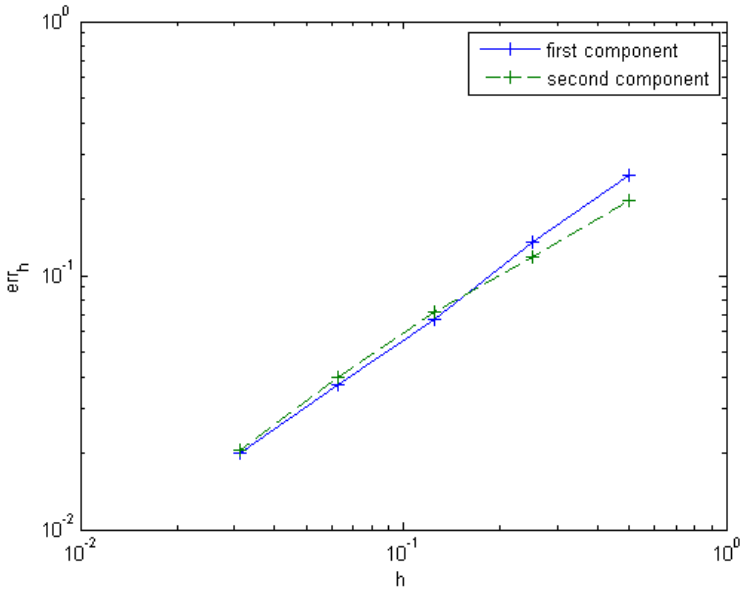

Figure 4.2: The error at steady state of the vector problem plotted for $h = 1/2, 1/4, 1/8, 1/16, 1/32$. The x and the y axes are proportional to $\log_{10} h$ and $\log_{10}(\mathrm{err}_h)$, respectively.

Chapter 5

Finite volume method for the equation of radiative transfer

The discrete ordinate method, which was introduced in Section 3.1, is one of the first developed as well as simplest methods to discretise direction in directional dependent equations. This method suffers from a number of serious drawbacks, for instance from the ray effect or false scattering. Moreover, we cannot choose the directions arbitrarily, but rather we have to choose them along with their weights according to quadrature rules, in order to obtain better agreement with the exact solution.

These disadvantages do not perish, even if we discretise space by the finite volume method, instead of the finite difference method, which is the analogy of the discrete ordinate method in space. The natural step, which has already been taken, is to develop a complete finite volume scheme. All the mentioned drawbacks do not disappear completely, nevertheless their influence should at least decrease.

While the finite volume method has been a standard method for the spatial discretisasion for some time now, first applications to direction started to appear only two decades ago. In the present chapter, we will derive the finite volume scheme for the equation of radiative transfer in both space and direction for unstructured triangular partitions. We will consider only two spatial and one directional dimensions. The finite volume method for radiative transfer equation in two dimensions was also derived and numerically tested by Kim and coworkers [8] and Modest [13].

5.1 Notation

Spectral radiance I is the unknown quantity in the equation of radiative transfer. In Chapter 2, we had 7-dimensional spectral radiance I, since we considered three spatial, two directional, one spectral and one temporal dimension. Here we consider only 2-dimensional space and direction, spectrum and time are each 1-dimensional. Again, we suppress the spectral dependence, since the radiative transfer equation is not coupled with respect to the spectral variable. Thus, we take only four dimensions of I into account. More often then not, we refer to spectral radiance only as radiance.

Whenever we do not explicitly show the dependence of I, we assume

$$I = I(\mathbf{r}, \varphi, t).$$

The symbol $\mathbf{r} \in \Omega$ is the location vector, $\varphi \in [0, 2\pi)$ is angle and $t \in (0, t_0]$ is time. Here Ω is a domain in $\mathbb{R}^2$ and $t_0 > 0$. Notice that we use angle φ instead of its associated unit directional vector $\mathbf{s}$ as the directional variable. Angle and its associated unit directional vector are related through

$$\mathbf{s}(\varphi) = \Big(s^x(\varphi),\ s^y(\varphi)\Big) = (\cos\varphi,\ \sin\varphi).$$

We will refer to the flux

$$\mathcal{P}\big(I, \varphi, \mathbf{n}\big) = \mathbf{s} \cdot \mathbf{n}\ I,$$

also as the physical flux to distinguish it from the numerical flux. The physical flux is the overall energy of particles traveling in the direction $\mathbf{s}$ that penetrate through a unit line segment perpendicular to $\mathbf{n}$ per unit time and unit angle.

We consider the spatial and temporal partitions defined in Section 4.1. We define the directional partition as a partition $0 = \varphi_0 < \varphi_1 < \ldots < \varphi_{M_\varphi} = 2\pi$ of the interval $[0, 2\pi]$ with the control angle $\Phi_m = (\varphi_m, \varphi_{m+1})$, such that the length of each control angle is lower or equal to π, i.e.

$$|\Phi_m| = |\varphi_{m+1} - \varphi_m| \leq \pi, \tag{5.1}$$

where $m \in \{0,\ 1,\ \ldots,\ M_\varphi - 1\}$. We introduce the last condition only to simplify further derivations. Its reason will be apparent later in this chapter. Furthermore, we denote a unit directional vector associated with φ_m by $\mathbf{s}_m$, that means

$$\mathbf{s}_m = \big(s_m^x,\ s_m^y\big) = \big(\cos\varphi_m,\ \sin\varphi_m\big),$$

where $m = 0, 1, \ldots, M_\varphi$. Let us note that Φ_m is not an angle, even though we call it the control angle.

5.2 Initial-boundary value problem

We shall consider the 2-dimensional version of the equation (2.11), the equation of radiative transfer, namely

$$\frac{1}{c}\frac{\partial I}{\partial t} + \mathbf{s}\cdot\nabla I = C(I), \tag{5.2}$$

with the collision term

$$C(I) = \sigma_{\mathrm{a}} B - (\sigma_{\mathrm{a}} + \sigma_{\mathrm{s}})I + \frac{\sigma_{\mathrm{s}}}{2\pi}\int_0^{2\pi} \Psi(\varphi', \varphi) I(\mathbf{r}, \varphi', t)\, d\varphi', \tag{5.3}$$

which is subject to the initial condition

$$I(\mathbf{r}, \varphi, 0) = I_0(\mathbf{r}, \varphi), \tag{5.4}$$

and the boundary condition

$$I(\mathbf{r}_b, \varphi, t) = b(\mathbf{r}_b, \varphi, t) \qquad \text{for} \quad \mathbf{s}\cdot\mathbf{n}_b < 0.$$

Here $\mathbf{r}_b \in \partial\Omega$ is the location and $\mathbf{n}_b$ is the outer normal of the boundary, c is the speed of light and I_0 and b are given functions. The boundary condition is prescribed only for incoming radiance. On the other hand if $\mathbf{s}\cdot\mathbf{n}_b \geq 0$, which means that I is outgoing, the radiation freely leaves the domain without further requirements. Modest [13] described more complicated boundary conditions for a number of reflective surfaces.

All the symbols in the collision term C are the same as in the equation (2.11) and described in Section 2.4. We have only substituted $\mathbf{s}$ for φ and $\mathbf{s}'$ for φ' and replaced the constant 4π with 2π, since in two dimensions the integral over all directions $\int_0^{2\pi} d\varphi$ is equal to 2π. Note that we must modify the scattering phase function Ψ accordingly to the substitution.

In vacuum, the collision term C is equal to zero. The equation (5.2) then becomes confusingly similar to the transport equation. The difference between the transport equation and the equation (5.2) with the zero right-hand side is that here $\mathbf{s}$ is not constant, but rather it depends on the directional variable φ. This makes a fundamental change in the way we solve (5.2) compare to the transport equation, as we also need to discretise the directional variable.

5.3 Temporal discretisation

First of all, we will discretise time by the Euler method. We integrate (5.2) over τ_k and approximate the integrals of the flux and the collision term by

the left endpoint rule, thereby getting the partially discrete scheme

$$\frac{1}{c}\left(I^{k+1}-I^{k}\right)+|\tau_k|\mathbf{s}\cdot\nabla I^{k}=|\tau_k|C(I^{k}), \tag{5.5}$$

where I^k is an approximation of I at time t_k, i.e.

$$I^{k}(\mathbf{r},\varphi)\approx I(\mathbf{r},\varphi,t_k).$$

Here $\mathbf{r}\in\Omega_i$ and $\varphi\in[0,2\pi)$. The initial condition is

$$I^{0}(\mathbf{r},\varphi)=I_0(\mathbf{r},\varphi), \tag{5.6}$$

and the boundary condition is

$$I^{k}(\mathbf{r}_b,\varphi)=b(\mathbf{r}_b,\varphi,t_k), \tag{5.7}$$

for $\mathbf{s}\cdot\mathbf{n}_b<0$.

5.4 Spatial and directional discretisation

In this section, we shall discretise space and direction both by finite volume method. Let us first note, that we use the notation and definitions developed in Section 4.1. Integrating the equation (5.5) and (5.6) over $\Omega_i\times\Phi_m$ we get

$$\frac{1}{c}\int_{\Phi_m}\int_{\Omega_i}\left(I^{k+1}-I^{k}\right)d\mathbf{r}\;d\varphi+|\tau_k|\int_{\Phi_m}\int_{\Omega_i}\mathbf{s}\cdot\nabla I^{k}\;d\mathbf{r}\;d\varphi=|\tau_k|\int_{\Phi_m}\int_{\Omega_i}C(I^{k})d\mathbf{r}\;d\varphi, \tag{5.8}$$

with the initial condition

$$\int_{\Phi_m}\int_{\Omega_i}I^{0}\;d\mathbf{r}\;d\varphi=\int_{\Phi_m}\int_{\Omega_i}I_0\;d\mathbf{r}\;d\varphi. \tag{5.9}$$

We rearrange the second double integral in (5.8) by employing Green's theorem as follows

$$\int_{\Phi_m}\int_{\Omega_i}\mathbf{s}\cdot\nabla I^{k}\;d\mathbf{r}\;d\varphi=\int_{\Phi_m}\int_{\partial\Omega_i}\mathbf{s}\cdot\mathbf{n}\;I^{k}\;d\ell\;d\varphi=\sum_{j\in N_i\cup N_i^b}\int_{\Phi_m}\int_{\ell_{ij}}\mathbf{s}\cdot\mathbf{n}_{ij}\;I^{k}\;d\ell\;d\varphi. \tag{5.10}$$

Let us remind that $\mathbf{n}$ is the outer normal of $\partial\Omega_i$ and $\mathbf{n}_{ij}$ the normal of ℓ_{ij}. Plugging (5.10) into the equation (5.8) and multiplying it by c, we obtain

$$\int_{\Phi_m}\int_{\Omega_i} I^{k+1}\ d\mathbf{r}\ d\varphi = \int_{\Phi_m}\int_{\Omega_i} I^k\ d\mathbf{r}\ d\varphi - c|\tau_k| \sum_{j\in N_i\cup N_i^b} \int_{\Phi_m}\int_{\ell_{ij}} \mathbf{s}\cdot\mathbf{n}_{ij}\ I^k\ d\ell\ d\varphi + c|\tau_k| \int_{\Phi_m}\int_{\Omega_i} C(I^k)\ d\mathbf{r}\ d\varphi. \tag{5.11}$$

We denote an approximation of the integral average of I^k over $\Omega_j \times \Phi_m$ or $\ell_j^b \times \Phi_m$ by $\bar{I}^k_{j,m}$, hence

$$\bar{I}^k_{j,m} = \begin{cases} \dfrac{1}{|\Phi_m||\Omega_j|} \displaystyle\int_{\Phi_m}\int_{\Omega_j} I^k(\mathbf{r},\varphi)\ d\mathbf{r}\ d\varphi & \text{for } j \in J, \\ \dfrac{1}{|\Phi_m||\ell_j^b|} \displaystyle\int_{\Phi_m}\int_{\ell_j^b} b(\mathbf{r},\varphi,t_k)\ d\mathbf{r}\ d\varphi & \text{for } j \in J^b. \end{cases} \tag{5.12}$$

At each time step t_k, we approximate radiance I^k by a piecewise constant function I_h^k such that $I_h^k = \bar{I}^k_{i,m}$ in the interior of each $\Omega_i \times \Phi_m$. The latter integral in (5.12) is introduced because we need two values of I_h^k on each edge ℓ_{ij}, out of which we compute numerical flux. For $j \in J^b$ however, ℓ_j^b lies on the boundary and so there is just one element adjacent to ℓ_j^b. We replace the integral average of the other element by the integral average of the boundary function.

The integral $\int_{\ell_{ij}} \mathbf{s}\cdot\mathbf{n}_{ij} I^k\ d\ell$ is the energy of particles penetrating through ℓ_{ij} per unit time and unit angle in the direction $\mathbf{s}$. We approximate the integral by means of the numerical flux $\mathcal{H}$, particular choice of which we discuss later. To be specific, we plug the values of the approximate solution I_h^k adjacent to ℓ_{ij} into $\mathcal{H}$, i.e.

$$\mathcal{H}\big(\bar{I}^k_{i,m}, \bar{I}^k_{j,m}, \mathbf{n}_{ij}\big) \approx \frac{1}{|\ell_{ij}|} \int_{\ell ij} \mathbf{s}\cdot\mathbf{n}_{ij}\ I^k\ d\ell. \tag{5.13}$$

Furthermore, we denote the integral of the numerical flux $\mathcal{H}$ over Φ_m as $\widehat{\mathcal{H}}_m$, thus

$$\widehat{\mathcal{H}}_m\big(\bar{I}^k_{i,m}, \bar{I}^k_{j,m}, \mathbf{n}_{ij}\big) \approx \frac{1}{|\ell_{ij}|} \int_{\Phi_m}\int_{\ell ij} \mathbf{s}\cdot\mathbf{n}_{ij}\ I^k\ d\ell\ d\varphi. \tag{5.14}$$

The integral on the right-hand side (excluding the preceding constant) is the energy of particles penetrating through ℓ_{ij} in all direction of the control angle Φ_m per unit time and $|\ell_{ij}|\widehat{\mathcal{H}}_m$ is the same quantity in the discrete scheme. We refer to $\widehat{\mathcal{H}}_m$ as the angular numerical flux.

To finalise our goal, we plug (5.14) and the first expression in (5.12) into (5.11), which together with (5.9) and the second expression in (5.12) gives the fully discrete scheme

$$\begin{aligned}
\bar{I}_{i,m}^{k+1} &= \bar{I}_{i,m}^{k} - \frac{c|\tau_k|}{|\Phi_m||\Omega_i|} \sum_{j \in N_i \cup N_i^b} \widehat{\mathcal{H}}_m\big(\bar{I}_{i,m}^{k}, \bar{I}_{j,m}^{k}, \mathbf{n}_{ij}\big) + c|\tau_k|\bar{C}_{i,m}^{k} && i \in J, \\
\bar{I}_{i,m}^{0} &= \frac{1}{|\Phi_m||\Omega_i|} \int_{\Phi_m} \int_{\Omega_i} I_0(\mathbf{r}, \varphi)\ d\mathbf{r}\ d\varphi && i \in J, \\
\bar{I}_{i,m}^{k} &= \frac{1}{|\Phi_m||\ell_i^b|} \int_{\Phi_m} \int_{\ell_i^b} b(\mathbf{r}, \varphi, t_k)\ d\mathbf{r}\ d\varphi && i \in J^b, \\
\bar{C}_{i,m}^{k} &= \frac{1}{|\Phi_m||\Omega_i|} \int_{\Phi_m} \int_{\Omega_i} C(I_h^k)\ d\mathbf{r}\ d\varphi, && i \in J.
\end{aligned} \tag{5.15}$$

Let us remind that $N_i \subset J$, $N_i^b \subset J^b$ and $J \cap J^b = \emptyset$.

5.5 Collision term and its integral average

To be able to apply the scheme (5.15), we need to approximate the two double integrals by a suitable numerical quadrature and express $\bar{C}_{i,m}^{k}$ and $\widehat{\mathcal{H}}_m$ in a more transparent form. Let us begin with the integral average $\bar{C}_{i,m}^{k}$. It is defined by

$$\bar{C}_{i,m}^{k} = \frac{1}{|\Phi_m||\Omega_i|} \int_{\Phi_m} \int_{\Omega_i} C(I_h^k)\ d\mathbf{r}\ d\varphi,$$

with the collision term (5.3), namely

$$C(I) = \sigma_{\mathrm{a}} B - (\sigma_{\mathrm{a}} + \sigma_{\mathrm{s}}) I + \frac{\sigma_{\mathrm{s}}}{2\pi} \int_0^{2\pi} \Psi(\varphi', \varphi) I(\mathbf{r}, \varphi', t)\ d\varphi'. \tag{5.16}$$

Since the approximate solution I_h^k is constant in each $\Omega_i \times \Phi_m$, the integration is fairly straightforward for isotropic scattering, $\Phi \equiv 1$. In this case, the

integral average $\bar{C}^k_{i,m}$ reads

$$\bar{C}^k_{i,m} = \sigma_{\mathrm{a}} B - (\sigma_{\mathrm{a}} + \sigma_{\mathrm{s}}) \bar{I}^k_{i,m} + \sigma_{\mathrm{s}} \sum_{n=0}^{M_\varphi - 1} \bar{I}^k_{i,n}. \tag{5.17}$$

In general, it is rather complicated to integrate the last term in (5.16), let us therefore deal with it first. We simplify the integral over the term as follows

$$\begin{aligned} \int_{\Phi_m} \int_{\Omega_i} \int_0^{2\pi} \Psi(\varphi', \varphi) I^k_h(\mathbf{r}, \varphi') \, d\varphi' \, d\mathbf{r} \, d\varphi &= \int_{\Phi_m} \int_{\Omega_i} \sum_{n=0}^{M_\varphi - 1} \int_{\Phi_n} \Psi(\varphi', \varphi) \bar{I}^k_{i,n} \, d\varphi' \, d\mathbf{r} \, d\varphi \\ &= |\Omega_i| \sum_{n=0}^{M_\varphi - 1} \bar{I}^k_{i,n} \int_{\Phi_m} \int_{\Phi_n} \Psi(\varphi', \varphi) \, d\varphi' \, d\varphi. \end{aligned}$$

Thus, the general formula for $\bar{C}^k_{i,m}$ reads

$$\bar{C}^k_{i,m} = \sigma_{\mathrm{a}} B - (\sigma_{\mathrm{a}} + \sigma_{\mathrm{s}}) \bar{I}^k_{i,m} + \frac{\sigma_{\mathrm{s}}}{2\pi} \sum_{n=0}^{M_\varphi - 1} \bar{I}^k_{i,n} \bar{\Psi}_{m,n}, \tag{5.18}$$

with

$$\bar{\Psi}_{m,n} = \frac{1}{|\Phi_m|} \int_{\Phi_m} \int_{\Phi_n} \Psi(\varphi', \varphi) \, d\varphi' \, d\varphi. \tag{5.19}$$

where the double integral needs to be either approximated with the aid of a sufficiently accurate numerical quadrature, or calculated exactly.

5.6 Angular numerical flux

The target of this subsection is to express the angular numerical flux $\widehat{\mathcal{H}}_m$ in a form that allows us to implement it directly as opposed to (5.14). To this end, we need to integrate the numerical flux over each control angle Φ_m. Consider the flux on a face ℓ_{ij} of a triangle Ω_i. The flux may be incoming in one part of the control angle and outgoing in the other. This is called the control angle overlap. This makes the integration more complicated and so it is a common practice to use the bold approximation. This means, that the flux is considered to be either incoming or outgoing the the whole control angle. Here, we will develop an exact treatment of the control angle overlap. Kim and coworkers [8] revise three types of manipulation of control angle overlap.

We have a scalar equation and so the physical flux

$$\mathcal{P}(I, \varphi, \mathbf{n}) = \mathbf{s} \cdot \mathbf{n}\ I$$

is also scalar. Therefore, its Jacobi matrix becomes an ordinary derivative. Moreover $\mathcal{P}$ is linear, hence its derivative P is constant with respect to I, i.e.

$$\mathrm{P}(\varphi, \mathbf{n}) = \frac{\partial \mathcal{P}(I, \varphi, \mathbf{n})}{\partial I} = \mathbf{s} \cdot \mathbf{n}.$$

We will use the numerical flux according to Steger-Warming scheme, see (4.4), i.e

$$\mathcal{H}(U, V, \mathbf{n}) = \mathrm{P}^+(\varphi, \mathbf{n})U + \mathrm{P}^-(\varphi, \mathbf{n})V,$$

which splits the numerical flux into the outgoing and incoming parts. Note that in this case, for a linear physical flux, the Steger-Warming numerical flux is equivalent to Vijayasundaram and Van Leer numerical fluxes. The positive and negative parts of P are defined by (4.3) and for a scalar equation they become

$$\mathrm{P}^+(\varphi, \mathbf{n}) = \max\big\{0,\ \mathrm{P}(\varphi, \mathbf{n})\big\},$$
$$\mathrm{P}^-(\varphi, \mathbf{n}) = \min\big\{0,\ \mathrm{P}(\varphi, \mathbf{n})\big\}.$$

Furthermore, we define

$$\Phi_m^+ = \Phi_m^+(\mathbf{n}) = \{\varphi \in \Phi_m : \mathrm{P}(\varphi, \mathbf{n}) < 0\}, \tag{5.20}$$
$$\Phi_m^- = \Phi_m^-(\mathbf{n}) = \{\varphi \in \Phi_m : \mathrm{P}(\varphi, \mathbf{n}) > 0\}. \tag{5.21}$$

Suppose we have an edge ℓ_{ij} of a triangle Ω_i with the outer normal $\mathbf{n}_{ij}$. The flux $\mathcal{P}(\varphi, \mathbf{n}_{ij})$ is outgoing in the set $\Phi_m^+(\mathbf{n}_{ij})$ and incoming in $\Phi_m^-(\mathbf{n}_{ij})$ with respect to Ω_i. If U and V are constant in Φ_m, then $\widehat{\mathcal{H}}_m$ satisfies:

$$\begin{aligned}\widehat{\mathcal{H}}_m(U, V, \mathbf{n}) &= \int\limits_{\Phi_m} \mathcal{H}(U, V, \mathbf{n})\ d\varphi = U \int\limits_{\Phi_m} \mathrm{P}^+(\varphi, \mathbf{n})\ d\varphi + V \int\limits_{\Phi_m} \mathrm{P}^-(\varphi, \mathbf{n})\ d\varphi \\ &= U \int\limits_{\Phi_m^+(\mathbf{n})} \mathrm{P}(\varphi, \mathbf{n})\ d\varphi + V \int\limits_{\Phi_m^-(\mathbf{n})} \mathrm{P}(\varphi, \mathbf{n})\ d\varphi. \end{aligned} \tag{5.22}$$

5.6.1 Incoming and outgoing angular numerical flux

Let us sum up what we have learnt so far. Thanks to (5.22) we can express the angular numerical flux $\widehat{\mathcal{H}}_m$ as

$$\widehat{\mathcal{H}}_m(\bar{I}_{i,m}^k, \bar{I}_{j,m}^k, \mathbf{n}_{ij}) = \bar{I}_{i,m}^k \int\limits_{\Phi_m^+} \mathbf{s} \cdot \mathbf{n}_{ij}\ d\varphi + \bar{I}_{j,m}^k \int\limits_{\Phi_m^-} \mathbf{s} \cdot \mathbf{n}_{ij}\ d\varphi. \tag{5.23}$$

It follows from (5.20) and (5.21) that $\mathbf{s} \cdot \mathbf{n}_{ij}$ is positive in $\Phi_m^+$and negative in Φ_m^-. Since $\widehat{\mathcal{H}}_m$ is subtracted in the scheme (5.15), the first term in (5.23) is the outgoing part and the second is the incoming part of the angular numerical flux with respect to Ω_i. Note that in this section we always assume $\Phi_m^\pm = \Phi_m^\pm(\mathbf{n}_{ij})$.

We can now substitute $\widehat{\mathcal{H}}_m$ in the finite-volume scheme (5.15). However, it is still unclear how to calculate the integrals on the right-hand side of (5.23). The next step therefore is to evaluate these integrals. Completing the dot product $\mathbf{s} \cdot \mathbf{n}_{ij}$ gives us

$$\int\limits_{\Phi_m^\pm} \mathbf{s} \cdot \mathbf{n}_{ij} \; d\varphi = n_{ij}^x \int\limits_{\Phi_m^\pm} s^x(\varphi) \; d\varphi + n_{ij}^y \int\limits_{\Phi_m^\pm} s^y(\varphi) \; d\varphi. \tag{5.24}$$

Let us remind that

$$\begin{aligned} \mathbf{s}(\varphi) &= \big(s^x(\varphi),\ s^y(\varphi)\big) = (\cos\varphi,\ \sin\varphi), \\ \mathbf{s}_m &= \big(s_m^x,\ s_m^y\big) = (\cos\varphi_m,\ \sin\varphi_m). \end{aligned}$$

We have defined the directional partition such that $|\Phi_m| \leq \pi$, see (5.1). Hence we have only the two following cases:

1. the numerical flux is either incoming, or outgoing in the whole interval $\Phi_m = (\varphi_m, \varphi_{m+1})$, or

2. there are two intervals $(\varphi_m, \varphi_{ij})$ and $(\varphi_{ij}, \varphi_{m+1})$, such that the numerical flux is incoming in one and outgoing in the other.

Before discussing each of the cases in more detail, we integrate s^x and s^y over each of the three intervals $(\varphi_m, \varphi_{m+1})$, $(\varphi_m, \varphi_{ij})$ and $(\varphi_{ij}, \varphi_{m+1})$. Let us start with $(\varphi_m, \varphi_{m+1})$:

$$\begin{aligned} \int\limits_{\Phi_m} s^x(\varphi) \; d\varphi &= \int\limits_{\varphi_m}^{\varphi_{m+1}} \cos\varphi \; d\varphi = \sin\varphi_{m+1} - \sin\varphi_m = s_{m+1}^y - s_m^y, \\ \int\limits_{\Phi_m} s^y(\varphi) \; d\varphi &= \int\limits_{\varphi_m}^{\varphi_{m+1}} \sin\varphi \; d\varphi = \cos\varphi_m - \cos\varphi_{m+1} = s_m^x - s_{m+1}^x. \end{aligned}$$

Similarly we integrate s^x and s^y over $(\varphi_m, \varphi_{ij})$ and $(\varphi_{ij}, \varphi_{m+1})$ and hence

obtain

$$\int_{\varphi_m}^{\varphi_{ij}} s^x(\varphi)\ d\varphi = s_{ij}^y - s_m^y, \qquad \int_{\varphi_m}^{\varphi_{ij}} s^y(\varphi)\ d\varphi = s_m^x - s_{ij}^x,$$
$$\int_{\varphi_{ij}}^{\varphi_{m+1}} s^x(\varphi)\ d\varphi = s_{m+1}^y - s_{ij}^y, \qquad \int_{\varphi_{ij}}^{\varphi_{m+1}} s^y(\varphi)\ d\varphi = s_{ij}^x - s_{m+1}^x.$$

If we now wish to substitute the integrals in the right-hand side of (5.24) for the obtained expressions, we need to know in which one of the intervals the numerical flux is incoming and in which one it is outgoing. To this end, we distinguish the four following cases:

(i) If $\mathbf{s}_m \cdot \mathbf{n}_{ij} \geq 0$ and $\mathbf{s}_{m+1} \cdot \mathbf{n}_{ij} \geq 0$, then

$$\Phi_m^+(\mathbf{n}_{ij}) = \Phi_m,$$
$$\Phi_m^-(\mathbf{n}_{ij}) = \emptyset,$$

and

$$\int_{\Phi_m^+} \mathbf{s} \cdot \mathbf{n}_{ij}\ d\varphi = n_{ij}^x\big(s_{m+1}^y - s_m^y\big) + n_{ij}^y\big(s_m^x - s_{m+1}^x\big),$$
$$\int_{\Phi_m^-} \mathbf{s} \cdot \mathbf{n}_{ij}\ d\varphi = 0.$$

(ii) If $\mathbf{s}_m \cdot \mathbf{n}_{ij} \leq 0$ and $\mathbf{s}_{m+1} \cdot \mathbf{n}_{ij} \leq 0$, then

$$\Phi_m^+(\mathbf{n}_{ij}) = \emptyset,$$
$$\Phi_m^-(\mathbf{n}_{ij}) = \Phi_m,$$

and

$$\int_{\Phi_m^+} \mathbf{s} \cdot \mathbf{n}_{ij}\ d\varphi = 0,$$
$$\int_{\Phi_m^-} \mathbf{s} \cdot \mathbf{n}_{ij}\ d\varphi = n_{ij}^x\big(s_{m+1}^y - s_m^y\big) + n_{ij}^y\big(s_m^x - s_{m+1}^x\big).$$

(iii) If $\mathbf{s}_m \cdot \mathbf{n}_{ij} > 0$ and $\mathbf{s}_{m+1} \cdot \mathbf{n}_{ij} < 0$, then

$$\begin{aligned}\Phi_m^+(\mathbf{n}_{ij}) &= (\varphi_m,\ \varphi_{ij}),\\ \Phi_m^-(\mathbf{n}_{ij}) &= (\varphi_{ij},\ \varphi_{m+1}),\end{aligned}$$

and

$$\begin{aligned}\int_{\Phi_m^+} \mathbf{s}\cdot\mathbf{n}_{ij}\ d\varphi &= n_{ij}^x\big(s_{ij}^y - s_m^y\big) + n_{ij}^y\big(s_m^x - s_{ij}^x\big),\\ \int_{\Phi_m^-} \mathbf{s}\cdot\mathbf{n}_{ij}\ d\varphi &= n_{ij}^x\big(s_{m+1}^y - s_{ij}^y\big) + n_{ij}^y\big(s_{ij}^x - s_{m+1}^x\big).\end{aligned}$$

Here φ_{ij} denotes the angle of the vector $\mathbf{s}_{ij} = (-n_{ij}^y,\ n_{ij}^x)$. In other words $s_{ij}^x = -n_{ij}^y = \cos\varphi_{ij}$ and $s_{ij}^y = n_{ij}^x = \sin\varphi_{ij}$.

(iv) If $\mathbf{s}_m \cdot \mathbf{n}_{ij} < 0$ and $\mathbf{s}_{m+1} \cdot \mathbf{n}_{ij} > 0$, then

$$\begin{aligned}\Phi_m^+(\mathbf{n}_{ij}) &= (\varphi_{ij},\ \varphi_{m+1}),\\ \Phi_m^-(\mathbf{n}_{ij}) &= (\varphi_m,\ \varphi_{ij}),\end{aligned}$$

and

$$\begin{aligned}\int_{\Phi_m^+} \mathbf{s}\cdot\mathbf{n}_{ij}\ d\varphi &= n_{ij}^x\big(s_{m+1}^y - s_{ij}^y\big) + n_{ij}^y\big(s_{ij}^x - s_{m+1}^x\big),\\ \int_{\Phi_m^-} \mathbf{s}\cdot\mathbf{n}_{ij}\ d\varphi &= n_{ij}^x\big(s_{ij}^y - s_m^y\big) + n_{ij}^y\big(s_m^x - s_{ij}^x\big).\end{aligned}$$

Here φ_{ij} denotes the angle of the vector $\mathbf{s}_{ij} = (n_{ij}^y, -n_{ij}^x)$. In other words $s_{ij}^x = n_{ij}^y = \cos\varphi_{ij}$ and $s_{ij}^y = -n_{ij}^x = \sin\varphi_{ij}$.

This finalises our goal in this subsection, as we have evaluated the integrals in (5.23) for each of the four cases, thereby calculating $\widehat{\mathcal{H}}_m$. We have also reached the main target of the whole chapter, since plugging (5.23) into (5.15) gives us the complete finite volume scheme for the equation of radiative transfer.

5.7 Finite volume scheme

We shall summarise our finite volume scheme for the equation of radiative transfer. Bringing (5.15), (5.18), (5.19) and (5.23) together gives us

$$\begin{aligned}
\bar{I}^{k+1}_{i,m} &= \bar{I}^{k}_{i,m} - \frac{c|\tau_k|}{|\Phi_m||\Omega_i|} \sum_{j \in N_i \cup N_i^b} \widehat{\mathcal{H}}_m\big(\bar{I}^{k}_{i,m}, \bar{I}^{k}_{j,m}, \mathbf{n}_{ij}\big) + c|\tau_k|\bar{C}^{k}_{i,m} && i \in J, \\
\bar{I}^{0}_{i,m} &= \frac{1}{|\Phi_m||\Omega_i|} \int_{\Phi_m} \int_{\Omega_i} I_0(\mathbf{r}, \varphi)\ d\mathbf{r}\ d\varphi && i \in J, \\
\bar{I}^{k}_{i,m} &= \frac{1}{|\Phi_m||\ell_i^b|} \int_{\Phi_m} \int_{\ell_i^b} b(\mathbf{r}, \varphi, t_k)\ d\mathbf{r}\ d\varphi && i \in J^b, \\
\bar{C}^{k}_{i,m} &= \sigma_{\mathrm{a}} B - (\sigma_{\mathrm{a}} + \sigma_{\mathrm{s}})\bar{I}^{k}_{i,m} + \frac{\sigma_{\mathrm{s}}}{2\pi} \sum_{n=0}^{M_\varphi - 1} \bar{I}^{k}_{i,n} \bar{\Psi}_{m,n}, && i \in J.
\end{aligned} \tag{5.25}$$

where

$$\bar{\Psi}_{m,n} = \frac{1}{|\Phi_m|} \int_{\Phi_m} \int_{\Phi_n} \Psi(\varphi', \varphi)\ d\varphi'\ d\varphi,$$

and

$$\widehat{\mathcal{H}}_m(\bar{I}^{k}_{i,m}, \bar{I}^{k}_{j,m}, \mathbf{n}_{ij}) = \bar{I}^{k}_{i,m} \widehat{\mathrm{P}}^{+}_{m}(\mathbf{n}_{ij}) + \bar{I}^{k}_{j,m} \widehat{\mathrm{P}}^{-}_{m}(\mathbf{n}_{ij}).$$

Here the functions $\widehat{\mathrm{P}}^{+}_{m}$ and $\widehat{\mathrm{P}}^{-}_{m}$ are as follows:

(i) For $\mathbf{s}_m \cdot \mathbf{n}_{ij} \geq 0$ and $\mathbf{s}_{m+1} \cdot \mathbf{n}_{ij} \geq 0$, we set

$$\begin{aligned}
\widehat{\mathrm{P}}^{+}_{m}(\mathbf{n}_{ij}) &= n^x_{ij}\big(s^y_{m+1} - s^y_m\big) + n^y_{ij}\big(s^x_m - s^x_{m+1}\big), \\
\widehat{\mathrm{P}}^{-}_{m}(\mathbf{n}_{ij}) &= 0.
\end{aligned}$$

(ii) For $\mathbf{s}_m \cdot \mathbf{n}_{ij} \leq 0$ and $\mathbf{s}_{m+1} \cdot \mathbf{n}_{ij} \leq 0$, we set

$$\begin{aligned}
\widehat{\mathrm{P}}^{+}_{m}(\mathbf{n}_{ij}) &= 0, \\
\widehat{\mathrm{P}}^{-}_{m}(\mathbf{n}_{ij}) &= n^x_{ij}\big(s^y_{m+1} - s^y_m\big) + n^y_{ij}\big(s^x_m - s^x_{m+1}\big).
\end{aligned}$$

(iii) For $\mathbf{s}_m \cdot \mathbf{n}_{ij} > 0$ and $\mathbf{s}_{m+1} \cdot \mathbf{n}_{ij} < 0$, we set $\mathbf{s}_{ij} = (-n^y_{ij},\ n^x_{ij})$ and

$$\begin{aligned}
\widehat{\mathrm{P}}^{+}_{m}(\mathbf{n}_{ij}) &= n^x_{ij}\big(s^y_{ij} - s^y_m\big) + n^y_{ij}\big(s^x_m - s^x_{ij}\big), \\
\widehat{\mathrm{P}}^{-}_{m}(\mathbf{n}_{ij}) &= n^x_{ij}\big(s^y_{m+1} - s^y_{ij}\big) + n^y_{ij}\big(s^x_{ij} - s^x_{m+1}\big).
\end{aligned}$$

(iv) For $\mathbf{s}_m \cdot \mathbf{n}_{ij} < 0$ and $\mathbf{s}_{m+1} \cdot \mathbf{n}_{ij} > 0$, we set $\mathbf{s}_{ij} = (n_{ij}^y, -n_{ij}^x)$

$$\widehat{\mathrm{P}}_m^+(\mathbf{n}_{ij}) = n_{ij}^x\big(s_{m+1}^y - s_{ij}^y\big) + n_{ij}^y\big(s_{ij}^x - s_{m+1}^x\big),$$
$$\widehat{\mathrm{P}}_m^-(\mathbf{n}_{ij}) = n_{ij}^x\big(s_{ij}^y - s_m^y\big) + n_{ij}^y\big(s_m^x - s_{ij}^x\big).$$

When all the values $\bar{I}_{i,m}^k$ are calculated, we can readily reconstruct the piecewise constant approximation I_h of I as follows

$$I_h(\mathbf{r}, \varphi, t) = \bar{I}_{i,m}^k \quad \text{for all } \mathbf{r} \in \Omega_i,\ \varphi \in \Phi_m,\ t \in \tau_k,$$

where $i \in J$, $m \in \{0, 1, \ldots, M_\varphi\}$ and $k \in \{0, 1, \ldots, M_t\}$.

Chapter 6

Numerical results

In this chapter, we shall first apply the scheme on a few test problems and then preform a test of convergence. The problems are designed merely to test the mathematical description of the method rather than to reconstruct real physical conditions with realistic coefficients. Are aim will be to examine how absorbing and scattering regions effect the solution.

In all the test problems, we assume that there is no surface on the boundary of the considered domain or that the boundary consists of the black surface (which both have the same consequences). All the outgoing radiation therefore freely leaves the boundary of the domain without being reflected.

Moreover, we consider isotropic scattering, $\Psi \equiv 1$, and replace the emission term $\sigma_{\mathrm{a}} B$ with a source term S in the radiation transfer equation (5.2). This means that we will be solving the equation

$$\frac{1}{c}\frac{\partial I}{\partial t} + \mathbf{s} \cdot \nabla I = S(\mathbf{r}, \varphi) - (\sigma_{\mathrm{a}} + \sigma_{\mathrm{s}}) I + \frac{\sigma_{\mathrm{s}}}{2\pi} \int_0^{2\pi} I(\mathbf{r}, \varphi', t)\ d\varphi', \tag{6.1}$$

in the following test problems. The reason for replacing the emission term is that we are not trying to reconstruct real physical conditions, therefore it does not make much sense to make up an artificial temperature field in order to fit are needs. Instead, we directly prescribe the emitted radiation. Let us notice, that now, when the phase function has disappeared, the integral on the right-hand has become irradiance $E = \int I\ d\varphi$.

Subsequent figures will plot irradiance rather than radiance for greater data transparency. We obtain an approximation of irradiance as follows

$$E_h = \int_0^{2\pi} I_h\ d\varphi = \sum_{m=0}^{M_\varphi - 1} |\Phi_m| I_h^k.$$

For more information about the relation between radiance I and irradiance E see Section 2.2.

The radiative transfer equation is linear and so the Courant-Friedrichs-Lewy condition, which we covered in Section 4.4, does not change in time. We therefore choose a uniform temporal partition. The expression (4.21), which is an approximation of the Courant-Friedrichs-Lewy condition, in the case of radiative transfer equation reads

$$|\tau| \leq \frac{d_i}{c(\cos\varphi + \sin\varphi)}, \tag{6.2}$$

for each $\varphi \in [0, 2\pi)$. The symbol d_i denotes the indiameter of Ω_i and c is still the speed of light. In general, the equation is coupled with respect to direction, therefore we must choose the same time step for all φ. We estimate the denominator as

$$\cos\varphi + \sin\varphi \leq \sqrt{2}.$$

This inequality is also the weakest possible estimate, as it becomes an equality for $\varphi = \pi/4 + k\pi/2$, where $k = 0, 1, 2, 3$. Taking this into account, we bind the time step to a particular spatial partition as follows

$$|\tau| = \min_{i \in J} \frac{d_i}{\sqrt{2}c}. \tag{6.3}$$

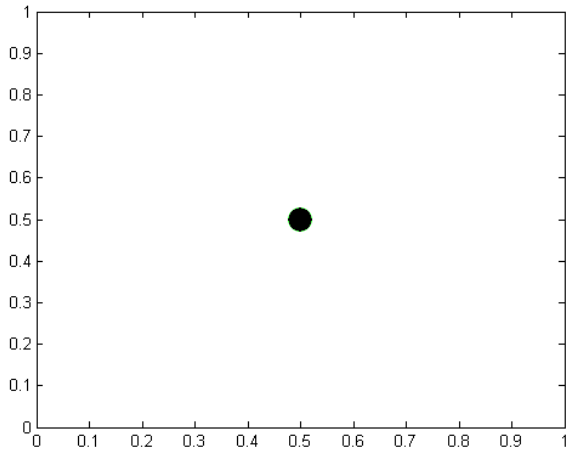

Figure 6.1: The flash of light. The initial function is $I_0 \equiv 6$ in the black circle with radius 0.03 and zero everywhere else. There are no absorbing, emitting or scattering regions nor are there any sources. There is no incoming radiation on the boundary.

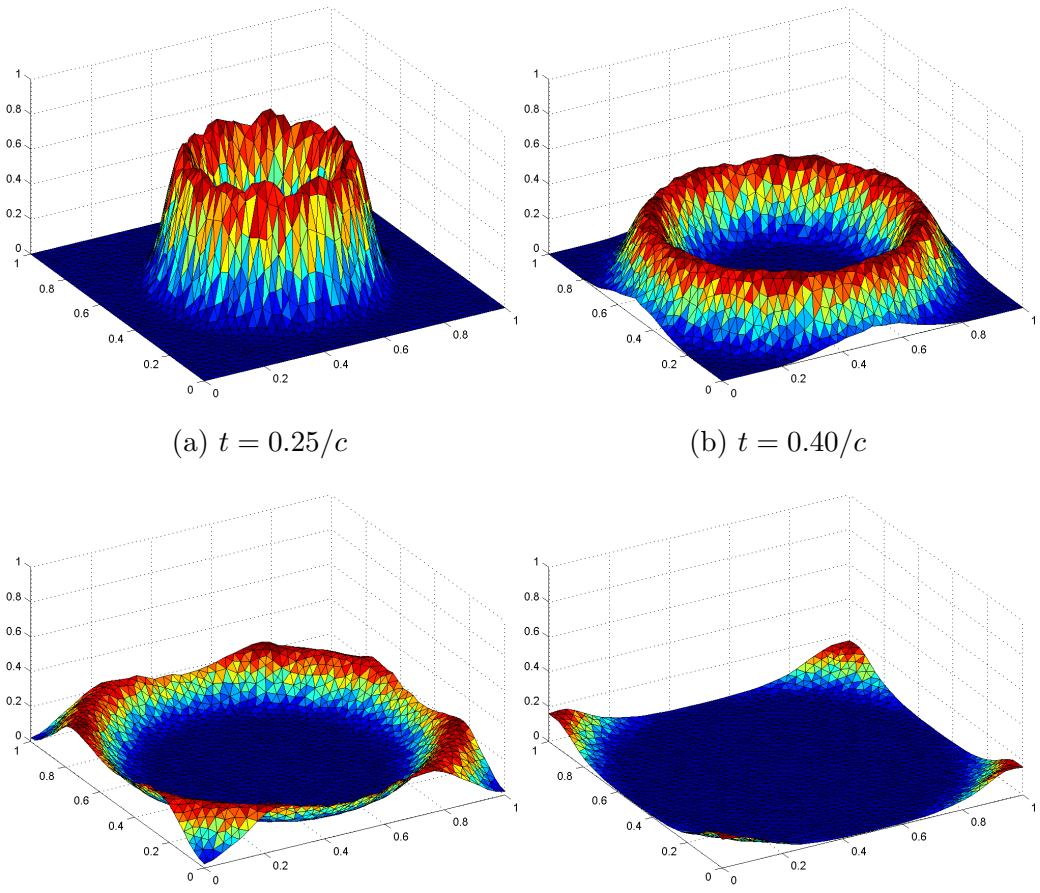

(a) $t = 0.25/c$ (b) $t = 0.40/c$

(c) $t = 0.55/c$ (d) $t = 0.70/c$

Figure 6.2: Irradiance E_h for the flash-of-light problem (see Figure 6.1) plotted at various times. The uniform directional partition with 32 control volumes was used.

6.1 Flash of light problem

We consider a strong impulse of electromagnetic radiation in a small circular region spreading in all directions equally. We assume no participating medium. Hence, we will be solving the equation of radiative transfer without the collision term. We choose the circular region to have the radius $r = 0.03$ and place it in the centre of the 1×1 square domain as shown in Figure 6.1. We simulate the impulse of electromagnetic radiation or the "flash of light" by setting the initial radiance $I \equiv 6$ in the circle. The chosen radiance is constant in direction, thus the electromagnetic radiation spreads in all directions equally.

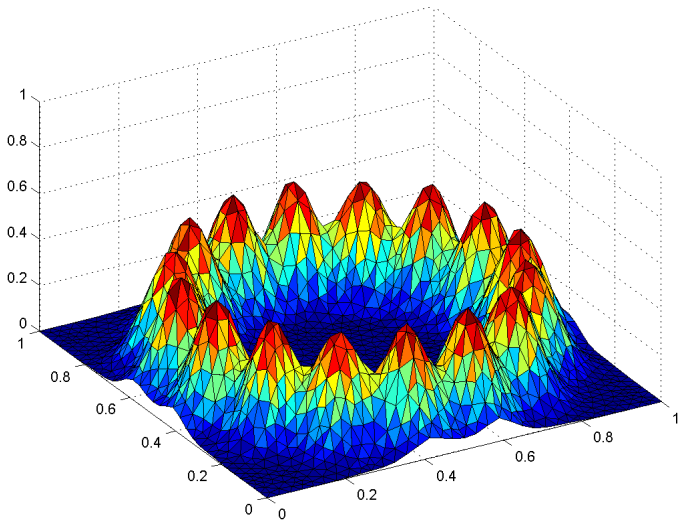

Figure 6.3: Irradiance E_h for the flash-of-light problem (see Figure 6.1) plotted at time $t = 0.40/c$. The uniform directional partition with 16 control volumes was used. Compare with Figure 6.2b.

The approximate solution was calculated using the uniform directional mesh with 32 control angles ($|\Phi_m| = \pi/16$) and spatial mesh with the maximum edge size $h = 0.03$. Approximate irradiance E_h is plotted in Figure 6.2. We can see that the approximate solution behaves more or less the way we would expect the exact solution to behave, except of course that the discontinuous initial condition is artificially smoothened by the inaccurate numerical treatment as time progresses.

Irradiance E_h computed for the same problem with unchanged spatial and directional partition, however with only 16 control angles instead of 32, is plotted in Figure 6.3 at time $t = 0.40/c$. Here, we can see the strong influence of the ray effect, which was almost absent in the previous test (compare with Figure 6.2b). As we discussed in Section 3.3.2, the ray effect can be reduced either by refining the directional partition, or by taking a coarser spatial mesh. The latter increases false scattering, which then compensates for the irregularities caused by the ray effect. For more information about false scattering see Section 3.3.1.

This means that when refining the spatial mesh, we need to refine the directional partition accordingly, to retain the balance between false scattering and the ray effect.

6.2 Bridge problem

This problem is designed to test absorbing regions. Again, we have the domain $\Omega = [0,1] \times [0,1]$. We consider a constant source of electromagnetic radiation on the right vertical line segment of the boundary, radiating in a small angle $\varphi \in [\pi - \pi/128,\ \pi + \pi/128]$. There are two pure absorbing regions present, as shown in Figure 6.4, otherwise there are no scattering or emitting regions. The initial function is identically equal to zero.

Since there is no scattering present, the system (5.25) is not coupled with respect to direction. As the only source of electromagnetic radiation is the boundary, radiance is nonzero only for $\varphi \in [\pi - \pi/128,\ \pi + \pi/128]$. Hence, we choose the uniform directional partition with ten control angles and

$$\varphi_0 = \pi - \pi/128,$$
$$\varphi_{M_\varphi} = \pi + \pi/128.$$

We take the same spatial and temporal partitions as before. We can see how the absorbing regions effect the solution in Figure 6.5.

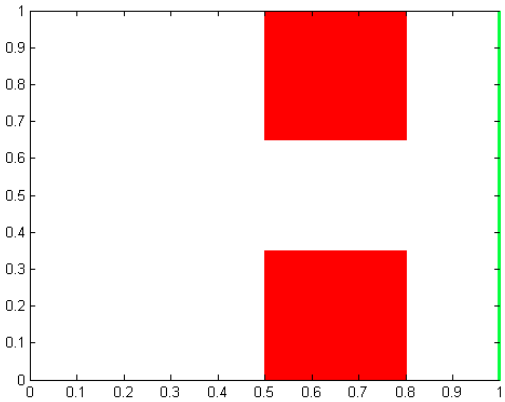

Figure 6.4: The bridge. The two red rectangles are pure absorbing regions with $\sigma_a = 2$, their hight is 0.35. The rest is vacuum. The boundary function is $b(\varphi, t) = 16$ for $\pi - \pi/128 \leq \varphi \leq \pi + \pi/128$ on the green part of the boundary, otherwise $b \equiv 0$. The initial function is $I_0 \equiv 0$.

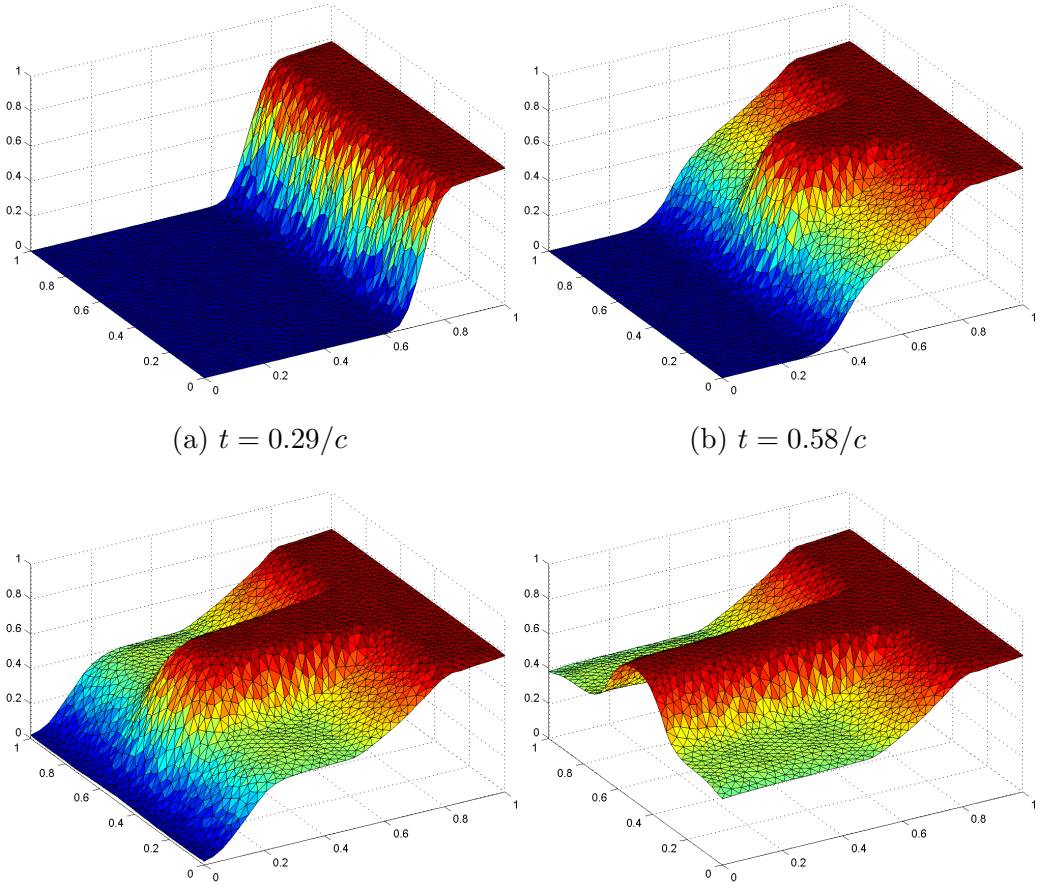

(a) $t = 0.29/c$ (b) $t = 0.58/c$

(c) $t = 0.87/c$ (d) $t = 1.16/c$

Figure 6.5: Irradiance E_h for the bridge problem (see Figure 6.4) plotted at various times. Figure 6.5d is the steady state.

6.3 Lattice problem

This problem is design to test how our solver deals with highly scattering as well as highly absorbing regions. We will recreate the exact same conditions as Brunner [1] used for his numerical experiment. The lattice system, depicted in Figure 6.6, contains eleven purely absorbing regions with $\sigma_\mathrm{a} = 10$, while the rest of the domain consist of purely scattering regions with $\sigma_\mathrm{s} = 1$. There are zero initial and boundary conditions. An isotropic source $S \equiv 1/(2\pi)$ is placed in the central region of the 7×7 square domain.

We simulate the radiative transfer for the source being turned on at time zero. Logarithmically scaled irradiance $\log_{10} E_h$ is shown in Figure 6.8 and Figure 6.7 at time $t = 3.2/c$. The results in Figure 6.8 were generated

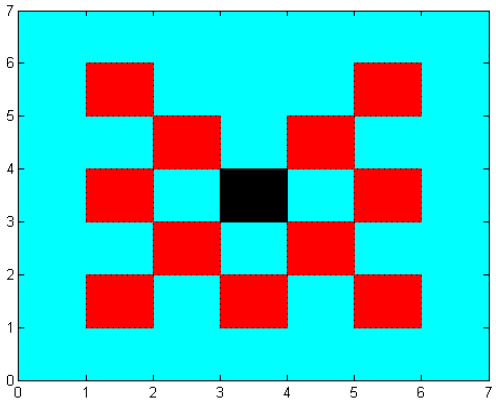

Figure 6.6: The lattice system. The red squares are pure absorbing regions with $\sigma_{\mathrm{a}} = 10$. The blue a black regions are pure scattering regions with $\sigma_{\mathrm{s}} = 1$. Moreover, the black region contains an isotropic source $S \equiv 1/(2\pi)$. There are zero initial and boundary conditions.

by a solver created by the author of the current thesis, according to the scheme (5.25), which is of course based on the finite volume method. Results in Figure 6.7 on the other hand were generated by solvers based on various methods, some of which we described in Chapter 3. These calculations were done by Brunner [1], who used his own solver for the P_N-approximations, while for the others he employed available solvers.

At time $t = 3.2/c$, the particles have just enough time to reach the boundary, but not the corners. In the diffusion approximation, shown in Future 6.7a, the particles clearly occupy the corners. We warned against this effect in Section 3.2.2. The Flux limited diffusion, in Figure 6.7b, is a significant improvement over the pure diffusion method, nevertheless there is not enough radiation leaking in between the absorbers. We have not covered this method in this thesis. In short, it is based on limiting the flux $\mathbf{F}$ in the diffusion method.

The particles in the P_1 calculation, Figure 6.7c, are way too slow. They travel at the speed of $c/\sqrt{3}$ instead of c. The S_6-approximation in Figure 6.7e shows an extensive influence of the ray effect. This method uses 24 directions and weights, since the order of quadrature N and the number of directions M for the discrete ordinate method are related through

$$M = \frac{1}{2}N^2 + N,$$

in two dimensions, see Table 3.1.

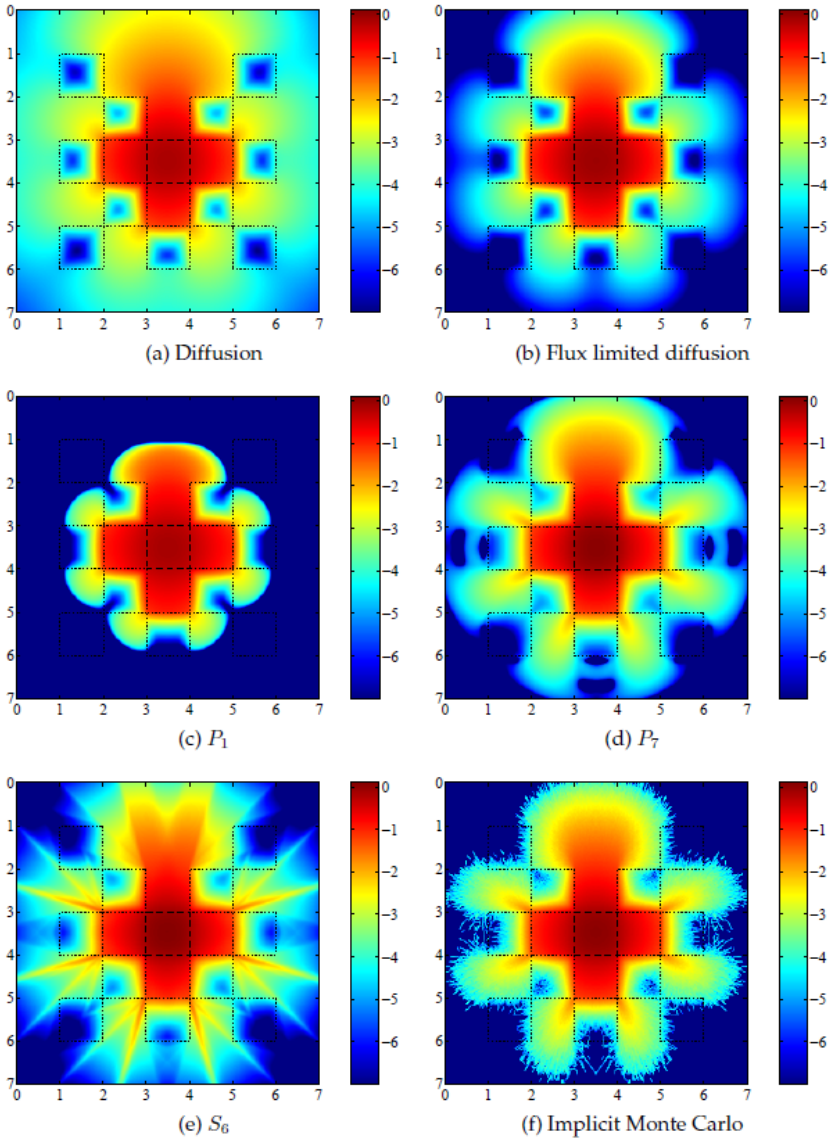

Figure 6.7: Simulation of the lattice problem calculated by various numerical methods and paused at time $t = 3.2/c$. The colour-map corresponds to $\log_{10} E_h$. These result were obtained by Brunner [1].

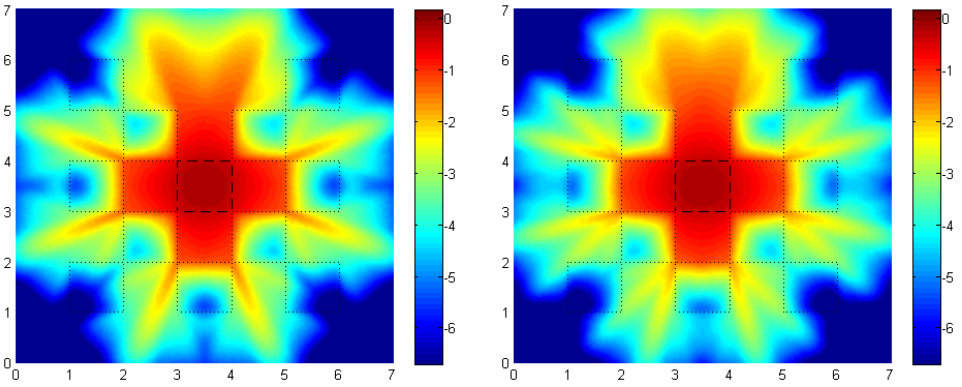

(a) $M_\varphi = 8$

(b) $M_\varphi = 12$

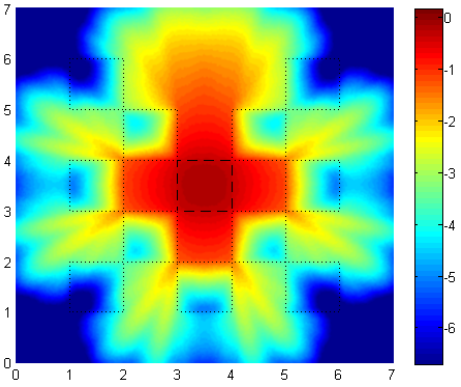

(c) $M_\varphi = 16$

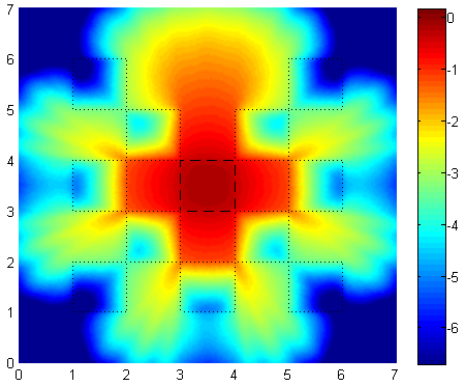

(d) $M_\varphi = 24$

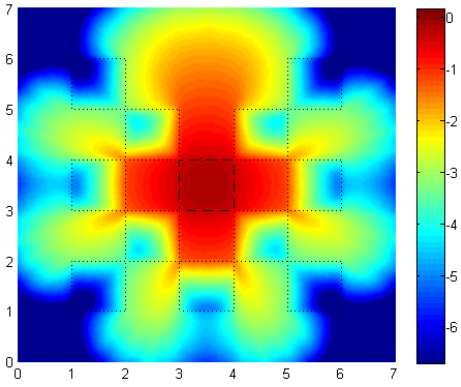

(e) $M_\varphi = 32$

Figure 6.8: Simulations of the lattice problem calculated by the finite volume method with M_φ control angles and paused at time $t = 3.2/c$. The colour-map corresponds to $\log_{10} E_h$.

The P_7 and implicit Monte Carlo simulations, shown in Figure 6.7d and Figure 6.7f, offer the most accurate results. They also agree with each other considerably well. They will be therefore helpful when evaluation our own results. The P_7 calculation however shows signs of the wave effect, which we discussed in Section 3.3.3. Monte Carlo is statistically based method that rely on repeated random sampling to obtain numerical results. We do not cover the description of this method in the present thesis.

To generate the results in Figure 6.8, we use a spatial mesh with $h = 0.05$ and four different uniform directional partitions with $M_\varphi = 8$, 12, 16, 24, where M_φ is the numbers of control angles. We can clearly see the ray effect in Figures 6.8a - 6.8c, and of course the less control angles, the stronger the effect. Let us take for instance Figure 6.8b, which uses 12 control angles. It quite obviously shows weaker influence of the ray effect than the discrete ordinate calculation (S_6) in Figure 6.7e, which uses 24 directions. To produce Figure 6.8d twenty-four control angles were used, but it shows considerably smoother behaviour than S_6. In fact, it very well agrees with the P_7 and Monte Carlo calculations, although it still shows a faint ray effect. The finest discretisation used, in Figure 6.8e, has barely any noticeable ray effect and matches with P_7 and Monte Carlo even better.

6.4 Test of convergence

We have applied the solver for a few test problem and it intuitively seems to be working correctly. In order to verify the right functioning of the solver more rigorously, we shall preform a test of convergence, just as we did for the direction-independent equation in Section 4.5. Let us first define the error and the residuum.

6.4.1 L_1-error and residuum

Again, we will be solving a steady-state problem. We end the calculation when the residuum

$$\mathrm{res}_k = \int_{\Omega_h} \left| E_h(\mathbf{r}, t_k) - E_h(\mathbf{r}, t_{k-1}) \right| \, d\mathbf{r} = \sum_{m=0}^{M_\varphi} |\Phi_m| \sum_{i \in J} |\Omega_i| \left| \bar{I}_{i,m}^k - \bar{I}_{i,m}^{k-1} \right|,$$

drops below 10^{-4}. Let $K \in \mathbb{N}_0$ be the smallest number such that $\mathrm{res}_K < 10^{-4}$. We consider approximate irradiance $E_h(\mathbf{r}, t_K)$ to be at steady state. As a

measure of accuracy, we take the L_1-error of irradiance at steady state, i.e.

$$\mathrm{err}_h = \sum_{i \in J} |\Omega_i| \big| E(\mathbf{r}_i) - E_h(\mathbf{r}_i, t_K) \big| \approx \int_{\Omega_h} \big| E(\mathbf{r}) - E_h(\mathbf{r}, t_K) \big| \, d\mathbf{r},$$

where $\mathbf{r}_i$ is the centroid of Ω_i as defined in (4.20). The rate of convergence is defined as follows

$$\mathrm{rate}_h = \log_2 \left(\frac{\mathrm{err}_{2h}}{\mathrm{err}_h} \right).$$

6.4.2 Inventing a solution

We need to compare the approximate solution generated by our solver with the exact solution of (6.1), which we do not know in general. Therefore we "invent" a solution and then calculate the source term S in order to fit the solution. Let us choose the domain $\Omega = [0, 1] \times [0, 1]$ and the exact solution

$$I(\mathbf{r}, \varphi) = \frac{1}{2\pi} \sin(\pi x) \sin(\pi y)(\cos \varphi + 1), \tag{6.4}$$

where $\mathbf{r} = (x, y)$. Now, we shall calculate the source term. As I does not depend on time, we have

$$\frac{\partial I}{\partial t} \equiv 0.$$

The gradient of I can be expressed as follows

$$\nabla I(\mathbf{r}, \varphi) = \frac{1}{2}(\cos \varphi + 1) \Big(\cos(\pi x) \sin(\pi y), \;\; \sin(\pi x) \cos(\pi y) \Big). \tag{6.5}$$

The integral in (6.1) is nothing else than irradiance

$$E = \int_0^{2\pi} I \; d\varphi = \sin(\pi x) \sin(\pi y). \tag{6.6}$$

We get the explicit formula for the source term S by plugging (6.4), (6.5) and (6.6) into

$$S = \mathbf{s} \cdot \nabla I + (\sigma_\mathrm{a} + \sigma_\mathrm{s}) I - \frac{\sigma_\mathrm{s}}{2\pi} E.$$

The chosen time-independent radiance I is equal to zero on the boundary $\partial\Omega$, thus we have the zero Dirichlet boundary condition for all $t > 0$. We

can take an arbitrary initial function. Let us choose the material coefficients as follows

$$\sigma_{\mathrm{a}} = \begin{cases} 1 & \text{for } x < 1/2, \\ 2 & \text{for } x > 1/2, \end{cases}$$

$$\sigma_{\mathrm{s}} = \begin{cases} 1 & \text{for } y < 1/2, \\ 2 & \text{for } y > 1/2. \end{cases}$$

6.4.3 Test of convergence for 16 control angles

Now, we solve (6.1) with the boundary function $b \equiv 0$, the initial function $I_0 \equiv 1/(2\pi)$ and the calculated source term, as if we did not know the exact solution. We will do so for five different spatial meshes with maximum edge size $h = 1/2$, $1/4$, $1/8$, $1/16$, $1/32$. We choose the uniform directional mesh with 16 control angles. Again, take the time step (6.3).

The error of irradiance E_h at steady state is plotted in Figure 6.9 and tabulated in Table 6.1 for each of the five meshes. The table also contains the number of time steps K_h that the solver took to obtain the solution and the convergence rate. The rate of convergence indicates linear convergence, which is just what we have been hoping.

h	K_h	err_h	rate_h
1/2	23	0.098	
1/4	38	0.0577	0.763
1/8	66	0.028	1.04
1/16	136	0.0134	1.06
1/32	241	0.00651	1.04

Table 6.1: The error, convergence rate and number of time steps at steady state for various values of h. Sixteen control angles were used here.

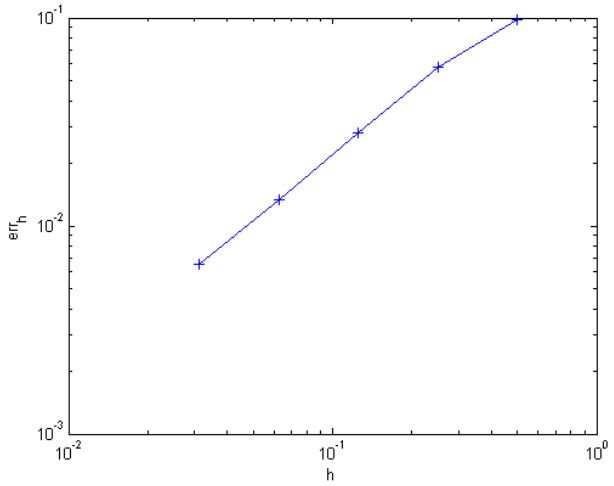

Figure 6.9: The error at steady state plotted for $h = 1/2$, $1/4$, $1/8$, $1/16$, $1/32$. Sixteen control angles were used here. The x and the y axes are proportional to $\log_{10} h$ and $\log_{10}(\mathrm{err}_h)$, respectively.

6.4.4 Test of convergence for 4 control angles

Even though we can be satisfied with the results for 16 control angles, we may wish to test the convergence rate for a courser directional discretisation. To this end, we choose the uniform partition with only four control angles, otherwise we keep the same settings. The results for this case are shown in Table 6.2 and Figure 6.10. Here, the solver converges linearly only up to $h = 1/8$. In the next step, the rate of convergence drops down. Eventually, the solver stops converging completely. The reason for this behaviour is clear. When refining the spatial and temporal partitions, the error caused by the spatial and temporal discretisation becomes eventually insignificant compare to the error due to the directional discretisation. Among others, the error caused by the directional approximation includes the discussed ray effect. Once again, these results remind us to keep the balance between the spatial and temporal discretisations on the one hand and the directional discretisation on the other.

h	K_h	err_h	rate_h
1/2	23	0.111	
1/4	40	0.0643	0.792
1/8	70	0.0312	1.04
1/16	143	0.0232	0.427
1/32	258	0.0247	−0.0915

Table 6.2: The error, convergence rate and number of time steps at steady state for various values of h. Four control angles were used here.

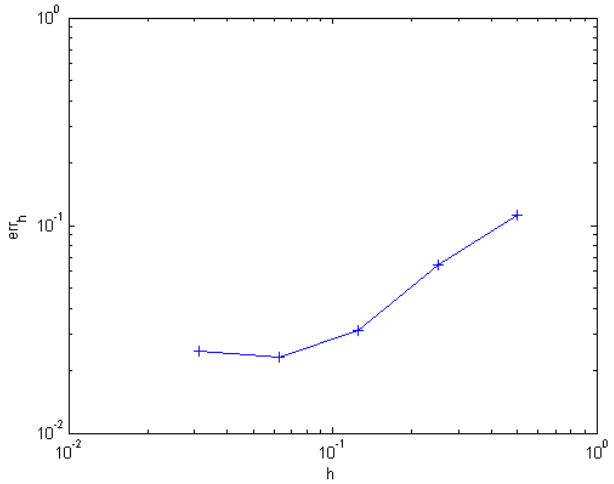

Figure 6.10: The error at steady state plotted for $h = 1/2$, $1/4$, $1/8$, $1/16$, $1/32$. Four control angles were used here. The x and the y axes are proportional to $\log_{10} h$ and $\log_{10}(\mathrm{err}_h)$, respectively.

Chapter 7

Conclusion

The central theme of the current thesis revolves around the equation of radiative transfer and its approximation. We concentrated especially on directional discretisation, as directional dependence is rather rare among partial differential equations. The discrete ordinate method could have been employed for this purpose. This method is simple, however it suffers from a number of defects such as the ray effect and false scattering. Despite their similarity, the finite volume method preforms better than the discrete ordinate method.

In an attempt to avert an unphysical numerical behaviour, we derived the finite volume method for unstructured spatial partitions and introduced an exact treatment of control angle overlap. In spite of our endeavours, the ray effect still occurs, as shown in the test problems; see Figure 6.3 or Figure 6.8. Nevertheless, the ray effect in the finite volume method is considerably weaker than that of the discrete ordinate method; compare Figure 6.7e and Figure 6.8. This is presumably because the former allows particles to travel in whole control angles whereas the latter just allows travel in specific directions. The finite volume method also conserves energy more efficiently than the discrete ordinate method.

For a reasonable number and distribution of control angles, the finite volume scheme derived in this thesis agrees considerably better with reality compared to the diffusion and P_1 calculations by Brunner [1]. Furthermore, flux limited diffusion, which is a substantial improvement upon the diffusion method, also performed worse than the finite volume solver. The best Brunner's results were obtained by the P_7 and Monte Carlo simulations. The finite volume solver should achieve a similar or higher level of accuracy for a sufficient number of control angles.

For a fixed number of control angles of a uniform partition the finite volume solver showed linear convergence when spatial and temporal partitions

were refined up to a certain point. The threshold, at which the solver stopped converging, depended on the number of control angles used. It would be considered a worthwhile attempt to derive a relationship which estimates where this singularity occurs for any given number of control angles. Since the ray effect increases as one moves away from the source, this derivation would presumably factor in the size of the domain.

Recommendations

This thesis is an introductory pursuit by the author to explore approximations of the radiation transport equation, and it is also the first example of literature on this subject at the local department of mathematics. There is, therefore, ample scope for further improvements and refinements. First and foremost, boundary conditions for reflective surfaces must be implemented into the scheme. Furthermore, an extension into three dimensions would broaden the scheme's applications. Finally, adding the material equation would make the scheme capable of solving real world physical problems.

The equation for radiative transfer depends on time, space and direction. In order to achieve higher accuracy with results, all three of these partitions would require refinement, and, as such, this is a costly endeavour. It is, therefore, desirable to rewrite the source code in a more efficient programing language, for instance ANSI C, C++, Fortran etc. Linear reconstruction of the finite volume method may also reduce the time of computation.

List of symbols and quantities

c	speed of light
c_0	speed of light in vacuum
n_c	refractive index
ν	frequency
λ	wavelength
η	wavenumber
h_{P}	Planck's constant
I	spectral radiance
E	spectral irradiance
$\mathbf{r}$	location vector variable
$\mathbf{s}, \mathbf{s}'$	unit directional vector variable
Ω, Ω'	solid angles associated with $\mathbf{s}$ and $\mathbf{s}'$ (in Chapters 2, 3)
B_λ, B_ν, B_η	Plank's function for various spectral variables
k_B	Boltzmann constant
t	time variable
σ_{a}	absorption and emission coefficient
σ_{s}	scattering coefficient
Ψ	scattering face function
$\otimes$	outer product
$\mathbf{F}$	radiative flux
$\mathbb{P}$	radiation pressure tensor
$\mathbf{s}_m$	unit directional vectors of the directional partition
w_m	quadrature weight associated with $\mathbf{s}_m$
Ω	domain in $\mathbb{R}^2$ (in Chapters 4, 5, 6)
$\partial\Omega$	boundary of Ω
Ω_h	piecewise linear approximation of Ω
$\mathcal{T}_h$	triangulation of Ω_h
Ω_i	control volume (element of $\mathcal{T}_h$)
J	set of indices of control volumes
h	maximum edge size of $\mathcal{T}_h$

ℓ_j^b	face of a control volume that is a part of the boundary
J^b	set of indices of the line segments above
ℓ_{ij}	either common face between Ω_i and Ω_j (if $j \in J$), or a face of Ω_i on $\partial\Omega_h$ (if $j \in J^b$)
$\mathbf{n}_{ij}$	outer normal of ℓij with respect to Ω_i
N_i	all the indices of neighbouring control volumes of Ω_i
N_i^b	set of indeces of faces of Ω_i that are part of the boundary
$t_0, t_1, \ldots$	nodes of the temporal partition
τ_k	time step $\tau_k = [t_k, t_{k+1}]$
$\mathcal{P}$	physical flux
$\mathbb{J}_{\mathcal{P}}$	Jacobi matrix of the physical flux
$\mathcal{H}$	numerical flux
$\mathbf{b}$	boundary functions
$\mathbf{r}_b$	location on the boundary
$\mathbf{r}_i$	centroid of Ω_i
$\mathbf{U}_i$	int. average of $\mathbf{u}$ over either Ω_i (if $i \in J$) or ℓ_i^b (if $i \in J^b$)
res_k	residuum at t_k
err_h	L_1-error at steady state
rate_h	convergence rate
K_h	number of time steps
φ	angular variable
$\mathbf{s}$	direction associated with φ
$\varphi_0, \varphi_1, \ldots$	angles of the directional partition
Φ_m	control angle
$\mathbf{s}_m$	direction associated with φ_m
C	collision term
$\bar{I}_{i,m}^k$	integral average of I over either $\Omega_i \times \Phi_m$ (if $i \in J$) or $\ell_i^b \times \Phi_m$ (if $i \in J^b$)
$\widehat{\mathcal{H}}$	angular numerical flux
$\Phi_m^+(\mathbf{n})$	subset of Φ_m in which $\mathcal{H}$ is outgoing from a finite volume with the outer normal $\mathbf{n}$
$\Phi_m^-(\mathbf{n})$	subset of Φ_m in which $\mathcal{H}$ is incoming into a finite volume with the outer normal $\mathbf{n}$
I_h	piecewise const. approximation of I on each $\Omega_i \times \Phi_m \times \tau_k$
E_h	piecewise constant approximation of E on each $\Omega_i \times \tau_k$

Bibliography

[1] T. A. Brunner: "Forms of Approximate Radiation Transport," Sandia Report (2002).

[2] S. Chandrasekhar: "Radiative Transfer," Dover Publications (1960).

[3] P. Cheng: "Dynamics of a radiating gas with application to flow over a wavy wall," AIAA Journal, vol. 4, no. 2, pp. 238-245 (1966).

[4] B. Davison: "Neutron Transport Theory," Oxford University Press (1958).

[5] M. Feistauer: "Theory and Numerics for Problems of Fluid Dynamics," (2006).

[6] H. Hensel, R. Iza-Teran, N. Siedow: "Deterministic model for dose calculation in photon radiotherapy," Phys. Med. Biol. 51 (2006).

[7] J. H. Jeans: "The equations of radiative transfer of energy," Monthly Notices Royal Astronomical Society, vol. 78, pp. 28-36 (1917).

[8] M. Y. Kim, S. W. Baek, J. H. Park: "Unstructured finite-volume method for radiative heat transfer in a complex two-dimensional geometry with obstacles," Numerical Heat Transfer, Part B, vol. 39, pp. 617-635 (2001).

[9] V. Kourganoff: "Basic Methods in Transfer Problems," Dover Publications (1963).

[10] C. E. Lee: "The discrete S_n approximation to transport theory," Los Alamos Scientific Laboratory of the University of California (1962).

[11] R. J. Leveque: Finite-volume methods for hyperbolic problems, Cambridge texts in applied mathematics (2002).

[12] U. M. Sultangazin, V. V. Smelov, A. S. Akisev, A. Sakabekov, I. Marek, S. Míka, K. Žitný: "Matematické otázky kinetické transportní teorie," Československá akademie věd (1986), (published in Russian language).

[13] M. F. Modest: "Radiative Heat Transfer," Second edition, Academic Press (2003).

[14] R. L. Murray: "Nuclear Reactor Physics," Engelwood Cliffs, Prentice Hall, NJ (1957).

[15] S. C. S. Ou and K. N. Liou: "Generalization of the spherical harmonic method to radiative transfer in multidimensional space," Journal of Quantitative Spectroscopy and Radiative Transfer, vol. 28, no. 4, pp. 271-288 (1982).

[16] G. C. Pomraning: "The equations of radiation hydrodynamics," Pergamon Press (1973).

[17] M. Sead, M. Frank, A. KlarCorresponding, R. Pinnau, G. Thmmes: "Efficient numerical methods for radiation in gas turbines," J. Comput. and Applied Mathematics, 170, pp. 217-239 (2004).

[18] http://www.mathworks.com.